General Disclaimer

One or more of the Following Statements may affect this Document

- This document has been reproduced from the best copy furnished by the organizational source. It is being released in the interest of making available as much information as possible.

- This document may contain data, which exceeds the sheet parameters. It was furnished in this condition by the organizational source and is the best copy available.

- This document may contain tone-on-tone or color graphs, charts and/or pictures, which have been reproduced in black and white.

- This document is paginated as submitted by the original source.

- Portions of this document are not fully legible due to the historical nature of some of the material. However, it is the best reproduction available from the original submission.

Prepared for

NATIONAL AERONAUTICS AND SPACE ADMINISTRATION

Headquarters
Washington, D.C. 20546

Dr. F. F. Marmo, Project Director and
Principal Investigator

September 1968

EXPERIMENTAL AND THEORETICAL STUDIES IN PLANETARY AERONOMY

Quarterly Progress Report

Covering the Period 24 May 1968 through
31 August 1968

Prepared under Contract No. NASW-1726

TABLE OF CONTENTS

I. INTRODUCTION

This first Quarterly Progress Report describes the technical progress achieved from 24 May 1968 through 31 August 1968 under NASA Contract No. NASW 1726. Scientific investigations accomplished during the reporting period resulted in the generation of the following papers submitted and/or accepted for publication in accredited scientific journals and/or GCA Technical Reports, or presented at scientific meetings.

Technical Papers Submitted and/or Accepted for Publication

a. Submitted	Publication
The Effect of Oxygen Cooling on Ionospheric Electron Temperatures (A. Dalgarno, et al)	Planet. and Space Sci.
Angular Distribution of Photoelectrons (J. A. R. Samson)	Phys. Rev.
Primary Processes in the Photolysis of SO_2 at 1849Å (P. Warneck, et al)	J. Chem. Phys.
Electron Impact Excitation of the Dayglow (A. Dalgarno, et als)	Planet. and Space Sci.
b. Published	
Photoelectron Spectroscopy of the Rare Gases (J. A. R. Samson, et al)	Phys. Rev., 173 81 (1968)
Scattering Cross Sections of Argon and Krypton in the VUV (J. A. R. Samson, et als)	J. Opt. Soc. Am. 58, (1968)
Photo-Attenuation Cross Sections of Xe and Xe_2 Between 1050 and 1550Å (Shardanand)	J. Quant. Spectrosc. Radiat. Transfer. 8, 1373 (1968)

In Section II, technical summaries are presented on the work performed during the current reporting period. Section III contains brief summaries of technical papers presented at scientific and/or professional meetings

as well as other miscellaneous topics of interest in the performance of the current contract committments. Finally, in compliance with the requirements of the contract, an integrated tabulation by labor category and grade of total hours expended in the execution of the contract, for the specified reporting time interval, is included in Section IV.

II. SUMMARY OF TECHNICAL WORK PERFORMED FOR THE PERIOD 24 MAY 1968 THROUGH 31 AUGUST 1968

The technical progress accomplished during the current reporting period can be conveniently described in terms of the two major categories contained in the statement of work: (A) laboratory studies, and (B) theoretical studies.

A. LABORATORY STUDIES

In accordance with the subject work statement, it is required to perform the following laboratory investigations on selected planetary atmospheric gases: (1) measure the absorption and photoionization cross sections for $\lambda\lambda < 500\text{Å}$, (2) measure the kinetic energies of photoelectrons generated by EUV photoionization, (3) acquire VUV ($\lambda\lambda$ 1050Å - 2000Å) high resolution absorption cross section data with emphasis on the minor constituents, (4) measure drift velocities and ionic mobilities, (5) measure rates of ion-neutral reactions, (6) measure the yield and kinetic energy of photoionization fragment ions, (7) acquire quantitative VUV photon scattering cross section data with emphasis on the spectral regions displaying discrete and/or continuous ionization and/or absorption features. In addition, measure the efficiency of resonance-fluorescence in these systems.

During the current quarterly reporting period, the bulk of the laboratory effort has been directed toward task items (1), (2), and (3) above. Brief descriptions of the progress achieved is given below in the order indicated.

1. Absorption and Photoionization Cross Sections of Planetary Gases for $\lambda\lambda < 500\text{Å}$.

The determination of quantative absorption and photoionization cross sections requires the capability of performing absolute intensity measurements in the spectral range of interest. Appropriate techniques have been devised and utilized in the VUV as demonstrated in this program. However, absolute intensity measurements for the EUV region involves a number of additional difficulties and constraints so that a number of modification must be applied to those techniques ordinarily employed in the VUV. The identification of the required modification and their application to this problem have been completed. The results achieved and their significance to the current task requirement are given below.

The rare gas ionization chambers provide the most direct method for measuring the absolute intensity of radiation of wavelengths less than 1000Å.[1,2] The principle of the ion chamber is simply that for every photon absorbed in the gas an ion pair is produced. Therefore, by measuring the number of ions produced, one immediately knows the number of photons absorbed. For total absorption, this number gives the value of the total intensity of the radiation. If the gas pressure is too low to absorb all of the photons, one can then use the known photoionization cross sections[3] to determine the fraction of photons absorbed. Again the measured ion current gives the absolute number of photons absorbed and hence the absolute intensity.

At present, the rare gas ion chambers have short-wavelength limit determined by the gas used. For He, it is about 300Å; for Ne, about

400Å; and for Ar, it is about 500Å. The reason for this limit is that for shorter wavelength the electrons are ejected with sufficient energy to cause secondary ionization. This gives a false value for the absolute intensity. In order to extend the use of the rare gas ionization chambers to shorter wavelength, it is therefore desirable to understand just how radiation is absorbed by the rare gases and to know the kinetic energies of the ejected photoelectrons. The total photoionization cross sections for the rare gases are known quite accurately, but we should know the specific cross sections for the ejecting electrons from the individual orbits. Some progress has now been made in this direction.[4]

Figure 1 illustrates the specific details of ionization which we might expect when Xe is photoionized by radiation of wavelength 460Å, that is, 27 eV. Electrons can be ejected from the outer p-shell leaving the residual ion in its ground $^2P_{3/2}$ state and in its excited $^2P_{1/2}$ state. There is also a finite probability that an inner s-shell electron will be ejected. When Xe is irradiated by a Flux of photons of 27-eV energy, each of these processes will take place with a definite probability and three grounds of electrons will emitted with different energies, namely, 14.9 eV, 13.6 eV, and 3.6 eV. By measuring the relative numbers of electrons within each group, one obtains the relative transition probabilities. In Figure 1, an imaginary curve is shown for a retarding potential type analyzer. The step-heights are directly proportional to the transition probabilities.

Figure 2 shows an actual curve when Ar is irradiated by 416.2Å. The step obtained for the ejection of an s-electron is clearly seen. How-

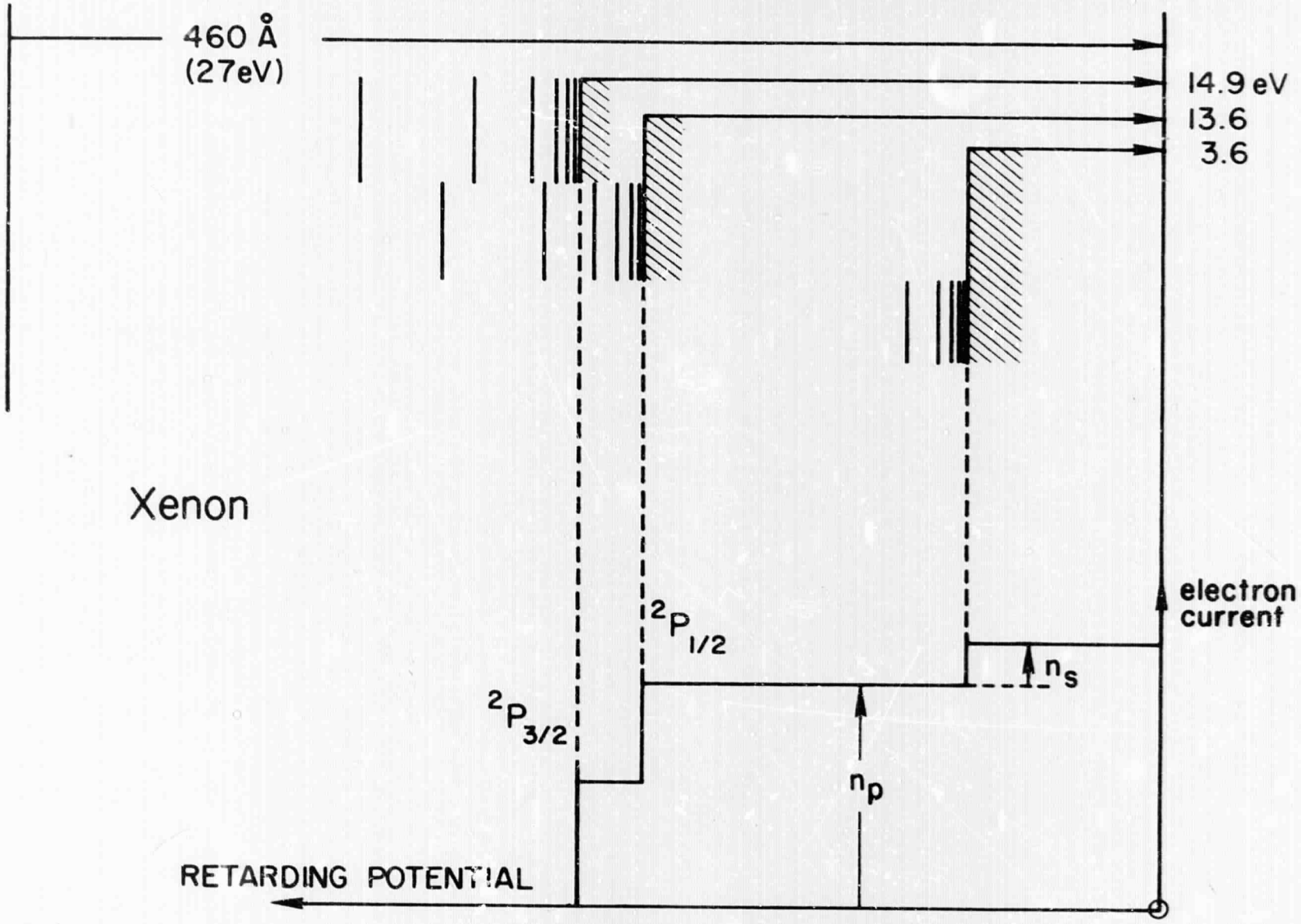

Figure 1. Specific details of the ionization of Xe by radiation of 460Å showing an imaginary retarding potential analysis of the energies of the ejected photoelectrons.

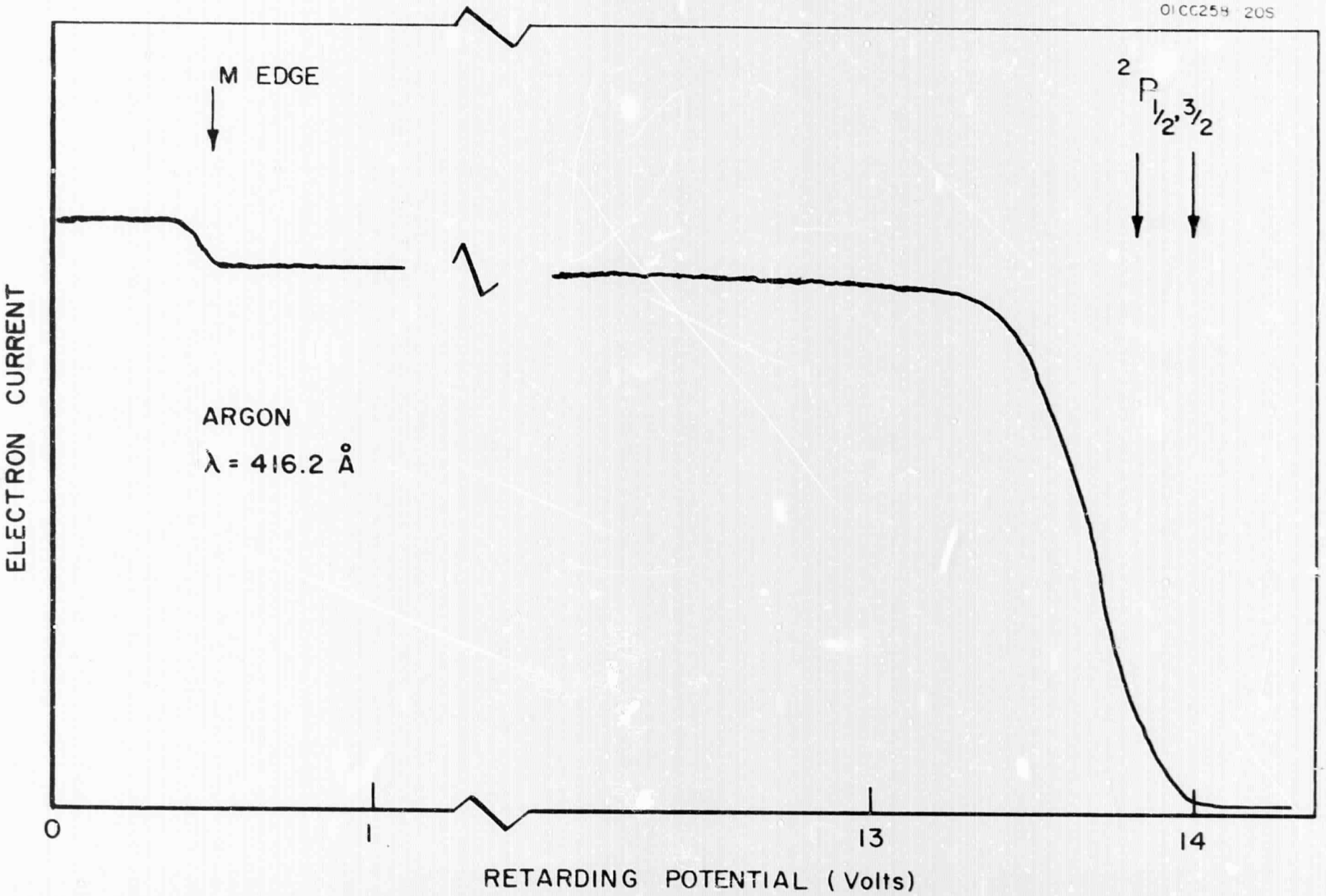

Figure 2. Retarding potential analysis of photoelectrons ejected from Ar at a wavelength 416.2Å. The step at 0.5 eV represents the ejection of s-electrons.

ever, the energy resolution of the retarding potential analyzer was not sufficient to resolve the $^2P_{1/2,3/2}$ edge for electrons of 14-eV energy. These two groups of electrons are separated by 0.178 eV. When a longer wavelangth is used to ionize Ar, this step can be resolved. Figure 3 was obtained at 735.9Å.

The analyzer used for this study is shown in Figure 4. Three concentric grids surround the ionizing volume which is obtained by channeling the incident radiation through two hollow cylinders which are separated by a small gap at the center of the spheres allowing the photoelectrons to escape. A retarding potential is applied between the inner and middle spheres. It is in this region that the energy of the electrons is analyzed. Any electrons, which are not retarded, are accelerated and focused onto the first dynode of an electron multiplier. The output of the multiplier plotted against the retarding potential gives data such as that shown in Figures 2 and 3. From the measured step-heights and the known total photoionization cross sections, one obtains the specific photoionization cross section for each of the different processes. Figures 5 and 6 give results of the specific cross sections for Ar and Xe, respectively.[4] The values shown for ejection of s-electrons are uncorrected for the instrumental discrimination of electrons of widely different energies and should be reduced by about a factor of seven.

Referring to Figure 7, we have seen that the cross section for ejecting an s-electron is very small in the region below the O_1-edge. Most of the electrons are p-electrons with energies about 15 eV. These electrons are energetic enough to cause secondary ionization. Hence, Xe

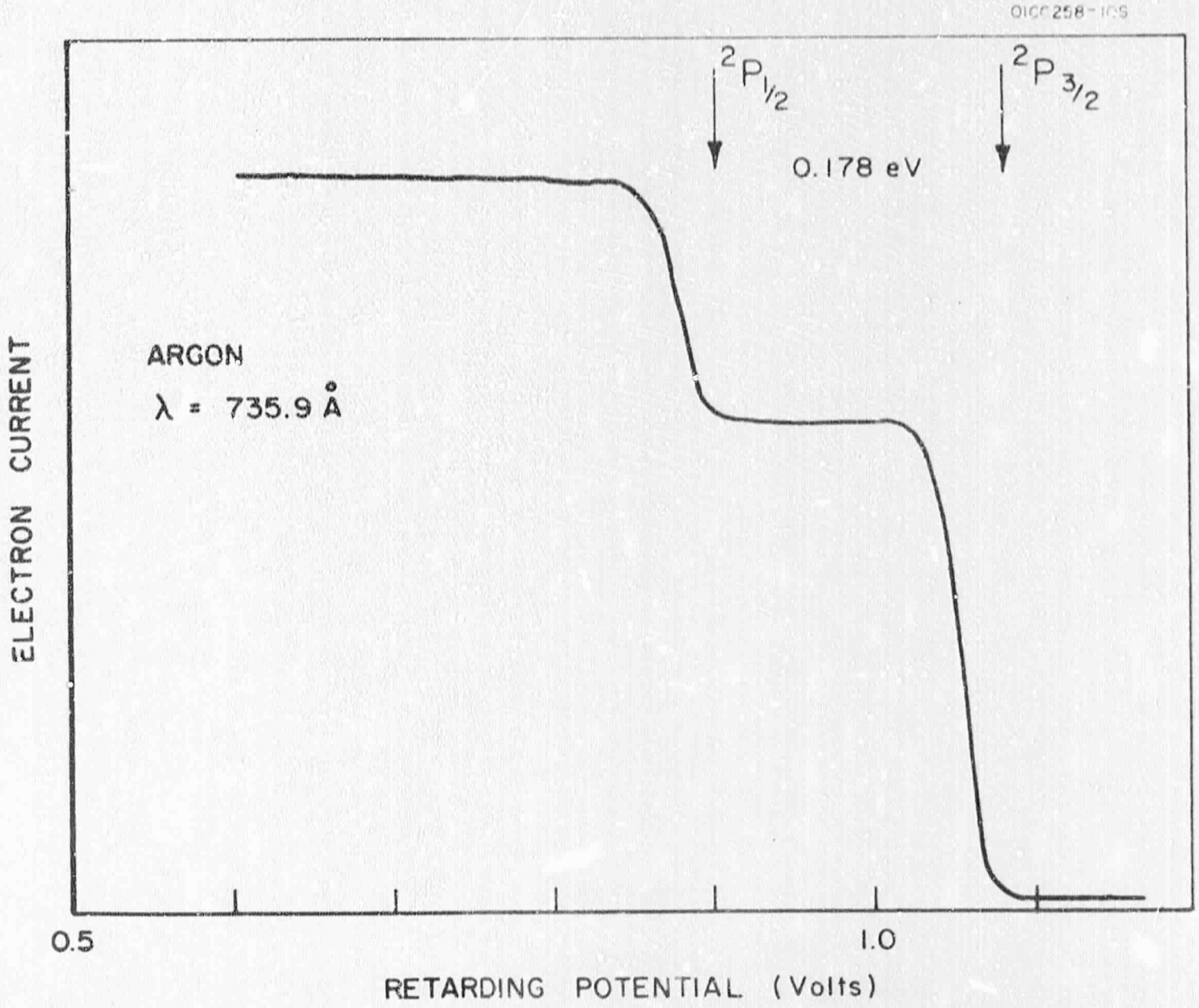

Figure 3. Retarding potential analysis of photoelectrons ejected from Ar at a wavelength of 735.9Å.

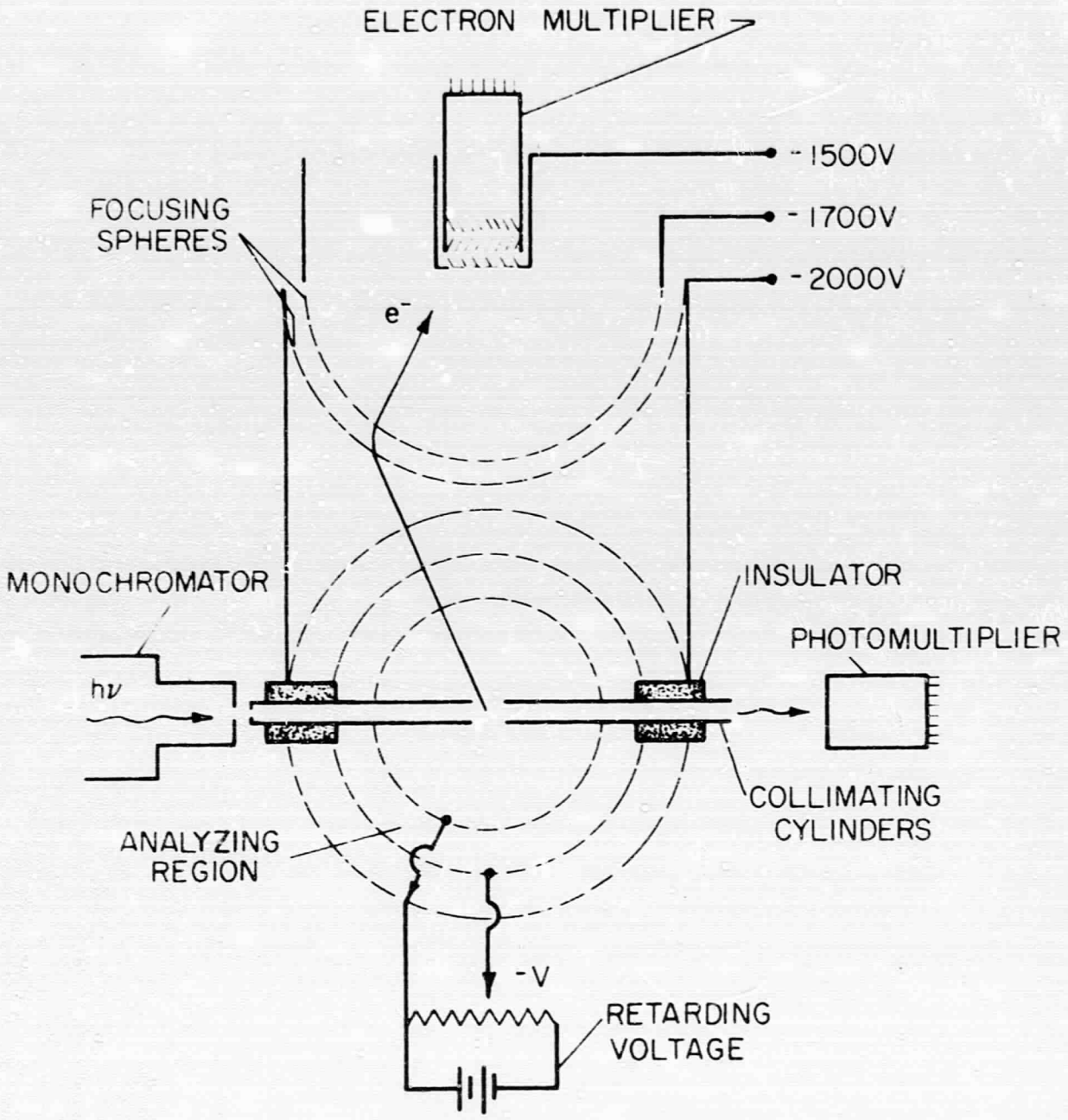

Figure 4. Spherical retarding potential analyzer

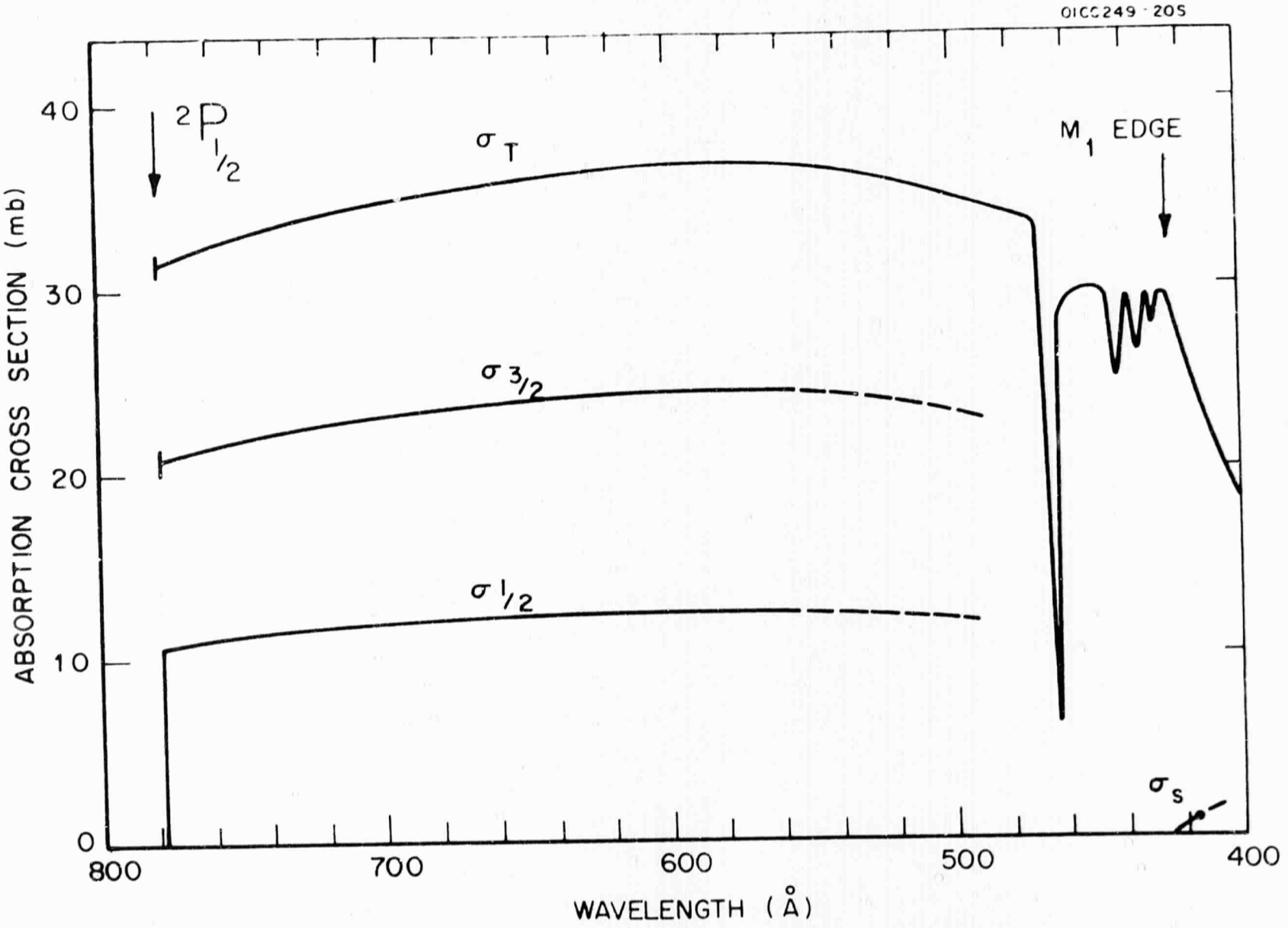

Figure 5. Specific photoionization cross sections for Ar.

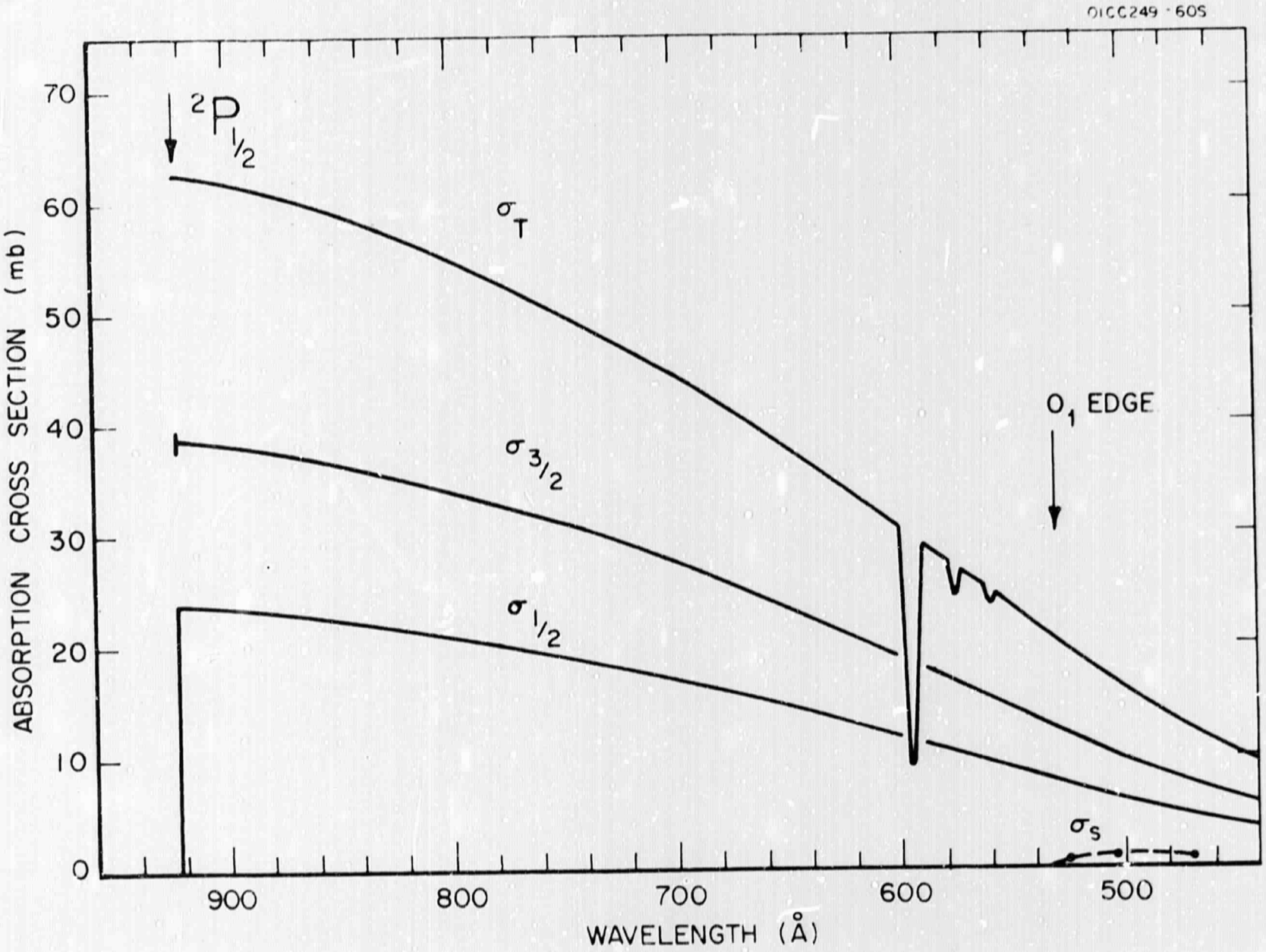

Figure 6. Specific photoionization cross sections for Xe.

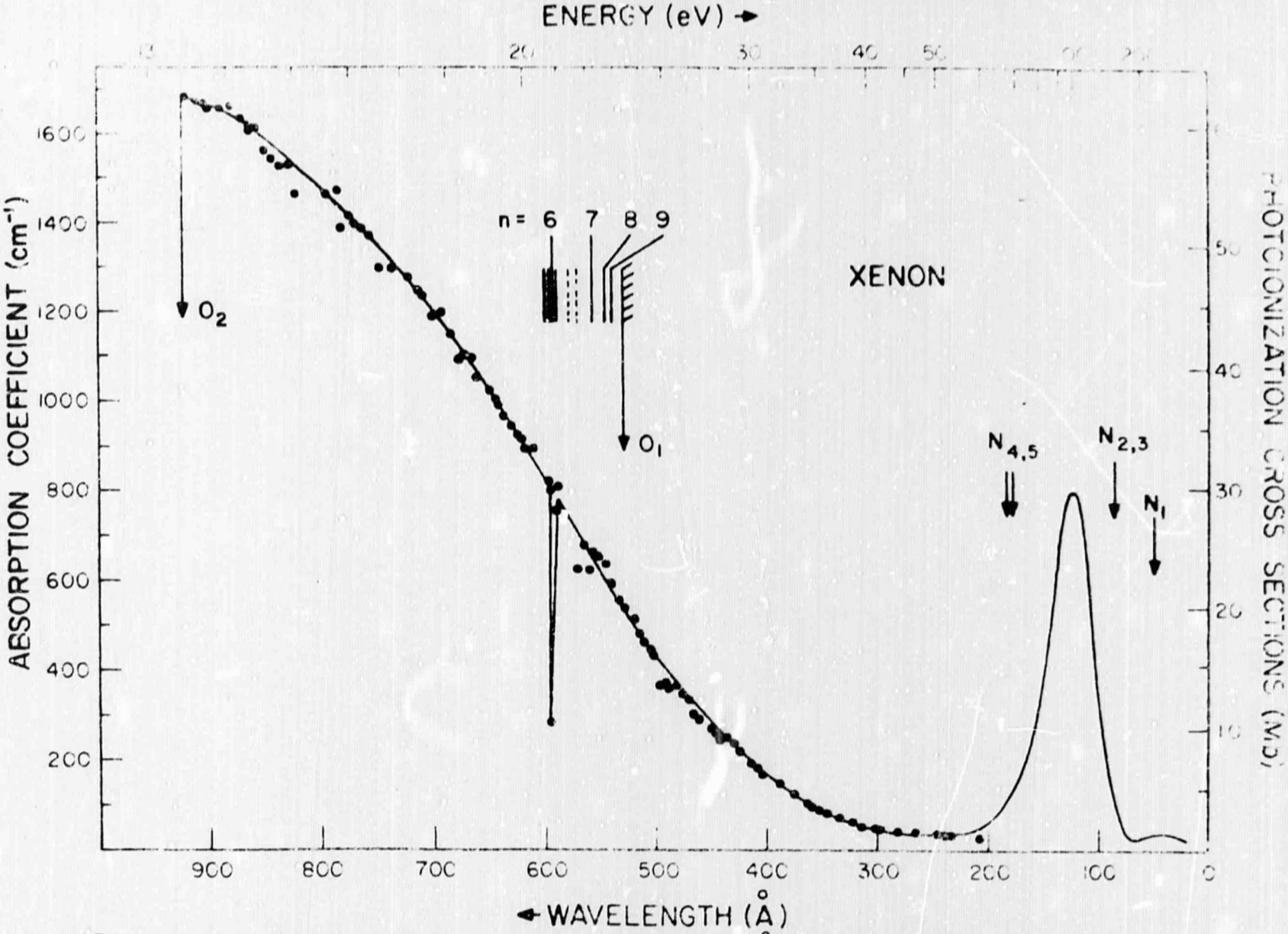

Figure 7: Total photoionization cross sections for Xe from the $^2P_{1/2}$ threshold to about 1Å

is not a suitable gas to use in an ion chamber for this wavelength region. We do not know the ratios of the s- to p-electrons in the region 200 to 300Å although theory predicts that the p-electrons are still about three times more abundant.[5] However, the interesting region is around 184Å. If this large cross-section peak is predominantly caused by ejection of d-electrons, then there is a band from the N-threshold at 184Å to about 160Å where the energy of the d-electrons is insufficient to cause ionization and would be a suitable region to measure absolute intensities. Figure 8 illustrates a similar band in Ar from 47.6 to 50.6Å.

As previously mentioned, helium is a suitable gas to use for measuring absolute intensities down to about 300Å before secondary ionization occurs. However, we have discovered a band between 270 and 252Å which does not cause secondary ionization. The reason for this band is different from those discussed for argon and xenon. When an ion chamber is used conventionally, one looks for a plateau in the ion current vs. voltage curve. A plateau occurs when the voltage is sufficient to retard all the electrons initially heading in the direction of the ion collector plate and continues until the electrons gain sufficient energy to cause secondary ionization. An example of such a plateau is shown in Figure 9. With helium this plateau becomes smaller and smaller as we approach 300Å, then it disappears. At this wavelength, the energy of the photoelectrons added to that of the applied field is sufficient to cause secondary ionization. However, below 300Å at the critical wavelength of 270.7Å the plateau reappears. At this wavelength, the ejected electrons can excite helium. At helium pressures of the order of 1 or 2 torr, this process occurs before

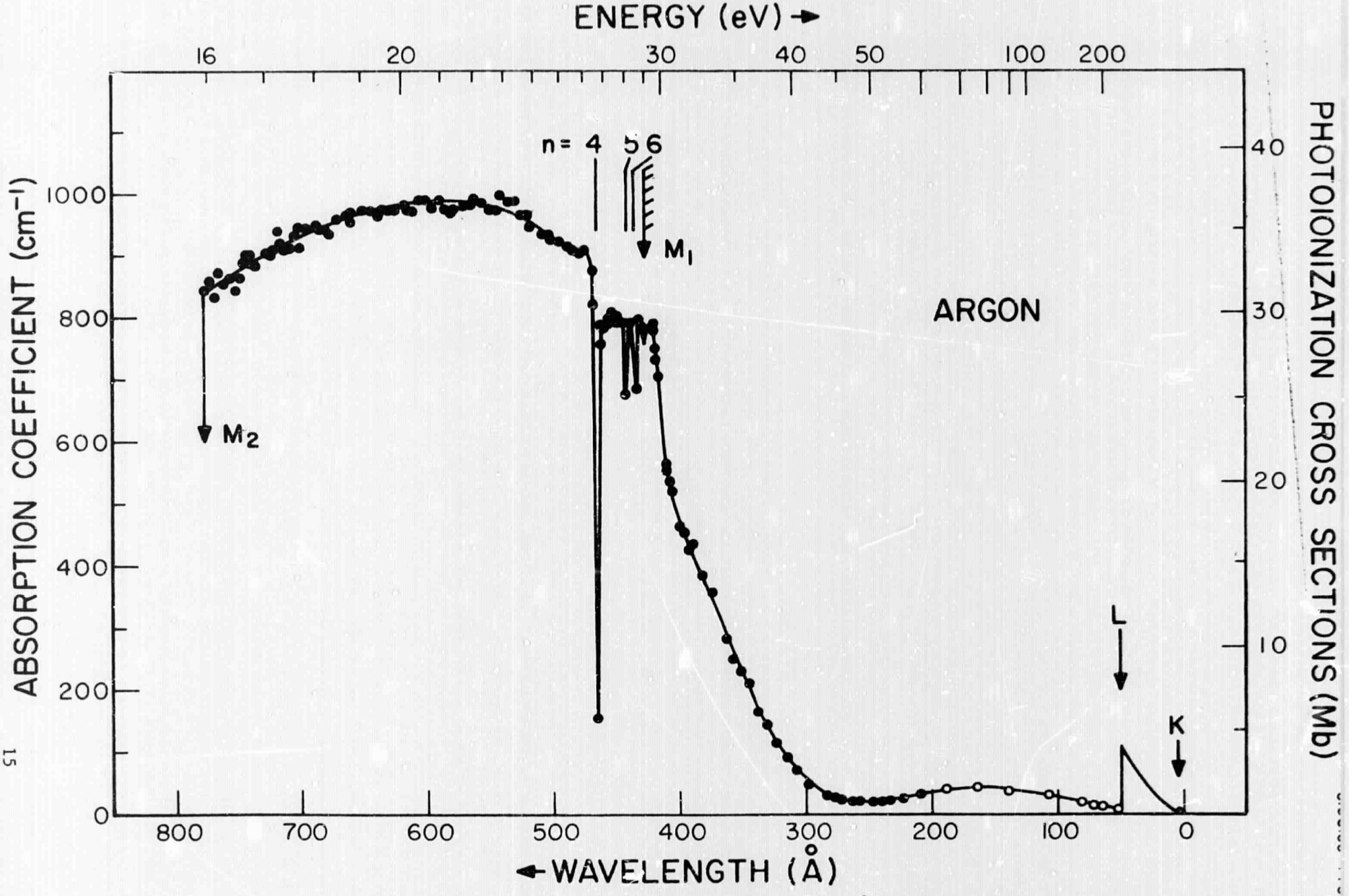

Figure 8. Total photoionization cross sections for Ar from $^2P_{1/2}$ threshold to about 1Å.

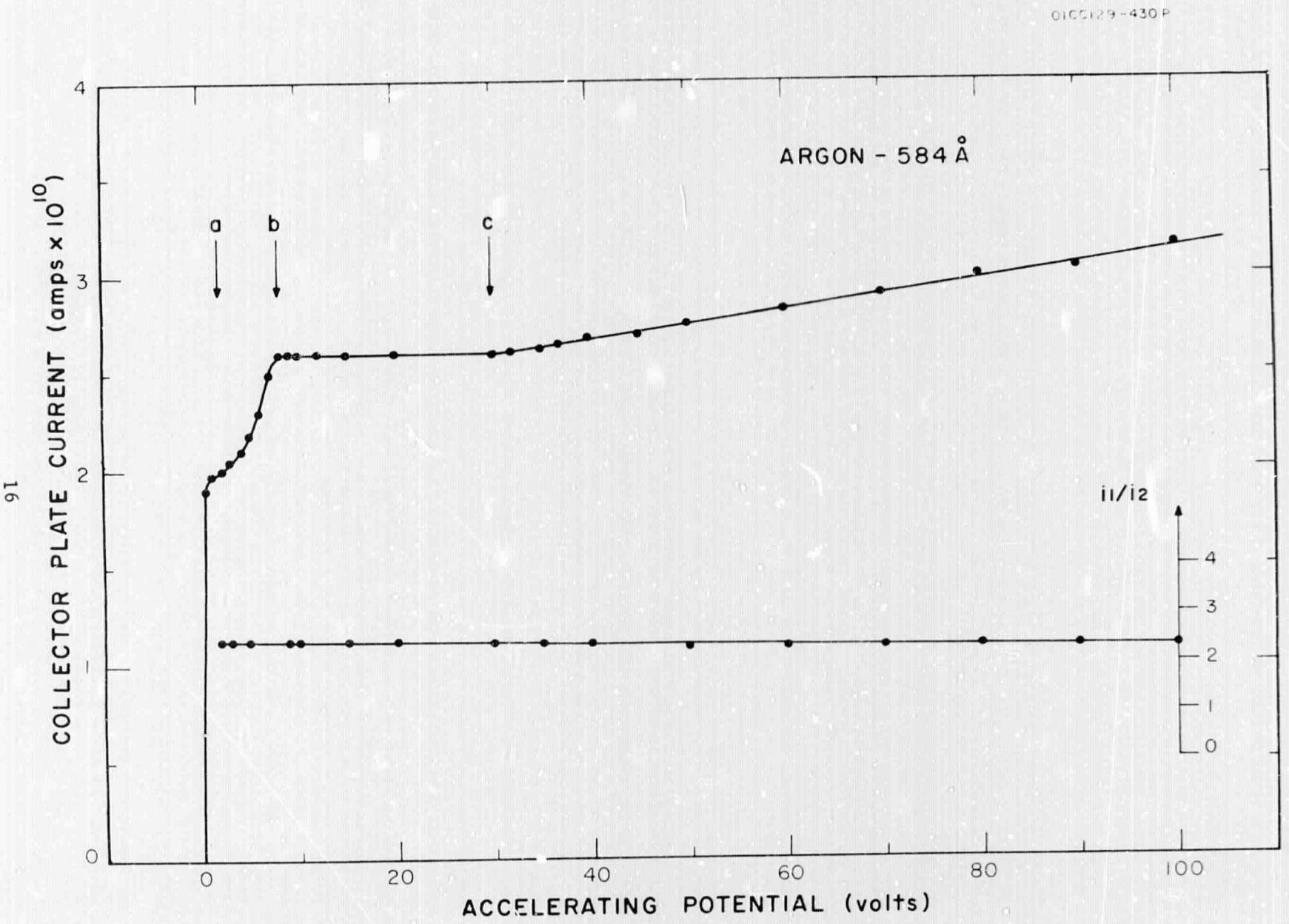

Figure 9: Ion chamber current as a function of the collector voltage illustrating the plateau region for absolute intensity measurements.

the electrons can gain sufficient energy from the applied field to ionize the gas. In fact, a low voltage can now be applied since the electrons lose most of their energy in exciting the helium and need not be retarded. The short-wavelength limit of this band is at 252.2Å. At this wavelength, the ejected photoelectrons can ionize the helium directly.

Let us look now at the possibility of using the rare gas ion chambers at any wavelength in the soft X-ray region. The main problem facing us is the production of secondary ions by the energetic photoelectrons. However, if we could use an ion chamber at a sufficiently low pressure such that the photoelectrons made extremely few collisions with the gas atoms, then the total ion current would be a good measure of the absolute intensity. However, at such low pressures the photoionization current may be too small to measure. If we set a lower limit on the detectable current and look for the best gas to use, that is, one which will have a high photoionization cross section (σ_{ph}) and a low-electron ionization cross section (σ_{el}) we arrive at the following:

$$\text{No. of secondary ions/photons} = C(\sigma_{el}/\sigma_{ph}) \qquad (1)$$

This formula is obtained by adjusting the gas pressure at each wavelength in order to give a constant primary photoionization current. Both cross sections vary with wavelength. σ_{el} varies with the electron energy which in turn depends on the wavelength. Figure 10 shows a plot of Equation (1) where C is determined by using the constant values of 10^{-14} amps for the primary current and $I_o = 10^6$ photons/sec for the pathlength of 76 cm. The values for the electron ionization cross sections were obtained from those published by Lotz.[6]

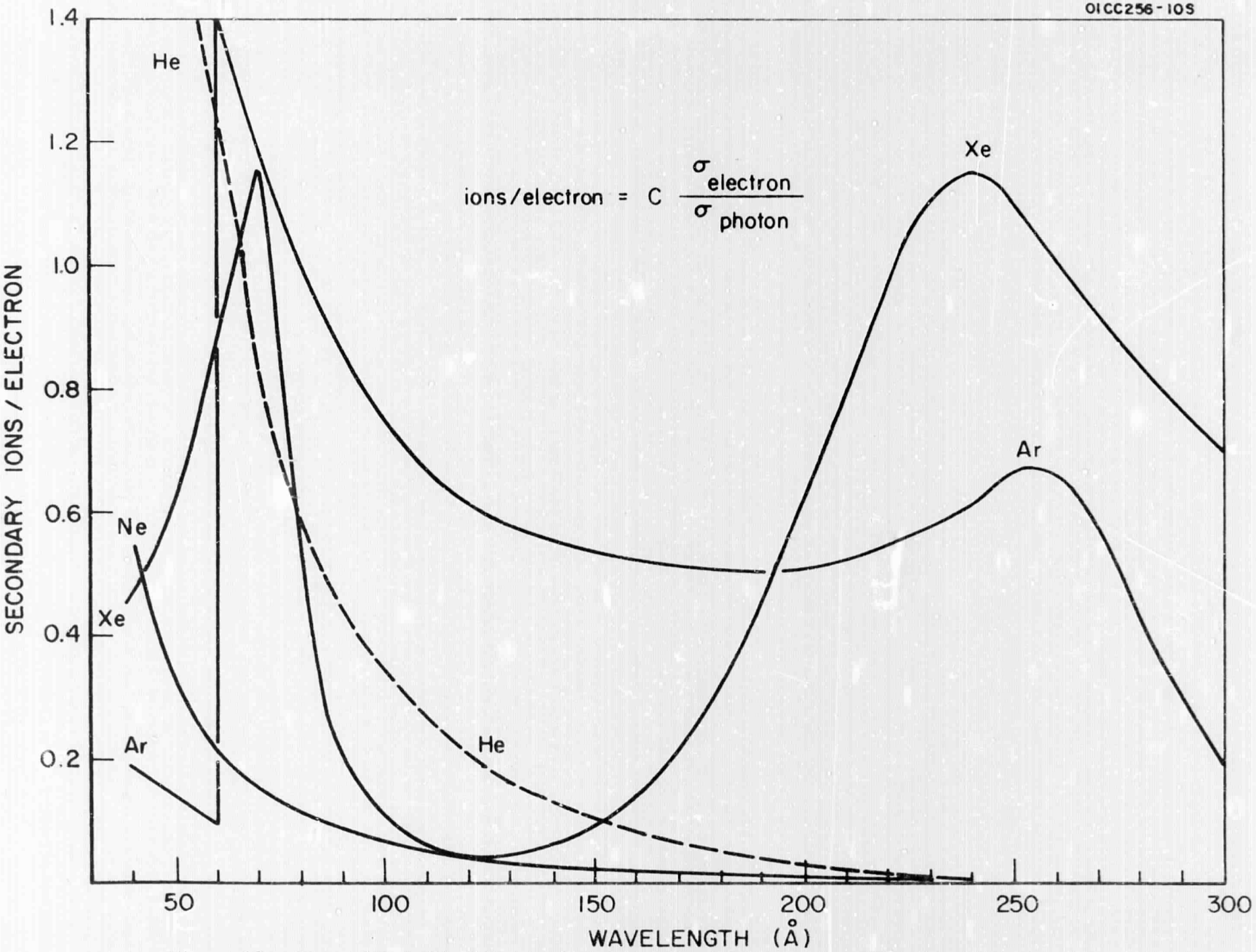

Figure 10: Plot of Eq. (1) illustrating the number of secondary ions produced as a function of wavelength for a variety of ion chamber gases.

It is interesting to note that neon and not helium produces the least number of secondary ions in the region 60 to 300Å. It appears possible, therefore, to use the rare gas ion chambers in the soft X-ray region when neon is used at low pressures. The secondary ion currents are small, but can be corrected for by using the published values for the electron ionization cross section.

2. Measurement of Kinetic Energy of Photoelectrons Generated by the EUV Photoionization of Planetary Gases

In the EUV photoionization of atmospheric gases, photoelectrons can be generated and released with appreciable kinetic energy. Theoretical aeronomy considerations[7,8] indicated that the initial energy distribution of these photoelectrons is an essential factor in establishing the steady state temperature of the electron gas in the upper atmosphere. These electron energy distribution data are also applicable to investigations on the escape of photoelectrons from the solar illuminated side toward the conjugated point on the night-side of the Earth.[8] In addition, there exists a requirement to measure the kinetic energy of electron yield associated with specific electronic vibrational energy states of pertinent atmospheric ions. This information is applicable to the interpretation of ion balance as well as to atmospheric airglow in any planetary atmosphere.

During the current quarter, two areas have been investigated (a) determination of higher ionization potentials of NO, CO and CO_2 by photoelectron spectroscopy, and (b) investigation on the determination of the angular distribution of photoelectrons.

a. Determination of Higher Ionization Potentials of NO, CO, and CO_2 by Photoelectron Spectroscopy

The required experimental capabilities for performing the tasks indicated has been developed at GCA under the present contract program. There is a continuing effort to improve the resolution and sensitivity capabilities of the techniques employed. Specifically, the present resolution capability amounts to about 0.1 eV. However, owing to the importance and

present requirement of appropriate data a number of gases were examined during the current quarterly reporting period in order to measure their photoelectron spectrum. Data have been acquired on the photoelectron spectrum of NO, CO and CO_2 for wavelengths of 469.8Å (26.39 eV) and 416.2Å (29.79 eV). At this point, only the basic data are available. Specifically for the case of NO, a higher ionization potential was observed at 21.57 eV. No level was found corresponding to the Tanaka α-series at 14.23 eV. However, an ionization potential was found at 15.52 eV. For CO and CO_2, no new ionization potentials were found up to the limiting photon energy of 29.79 eV. Mulliken has predicted a higher ionization potential for ejection of the 1σ electrons at an energy less than 32 eV. An analysis of these data is being performed; the detailed results will be reported in the next quarterly progress report.

b. Investigation on the Determination of Angular Distribution of Photoelectrons.

Most experiments, which measure the kinetic energies of photoelectrons, sample only those electrons ejected at right angles to the incident photon beam. Because the angular distribution of the ejected photoelectrons vary with their kinetic energy, angular momentum, and upon the varying degree of polarization of the incident photon beam, these measurements will not, in general, produce a true representation of the relative numbers of electrons within each energy group. However, it can now be shown that if observations are made at an angle of $54^{\circ}44'$ with respect to the direction of the incident beam and to the electric vectors of the two mutually orthogonal components comprising the partially polarized beam, a true representation is possible.

Transition probabilities for transitions from the ground-state to the ionic-state of atoms of molecules can be determined using the technique of photoelectron spectroscopy. This technique measures the kinetic energy of the ejected photoelectrons and the relative numbers of these electrons within each energy group. Knowing the relative numbers of electrons in each group and the total photoionization cross section at a specific wavelength, the transition probabilities at that wavelength can be obtained. However, it is important that the true representation of the relative numbers of electrons within each energy group is obtained.

Most experiments, which measure the kinetic energies of photoelectrons, sample only those electrons ejected at right angles to the incident photon beam.[9] The solid angle of acceptance by these analyzers is generally very small ($\approx 10^{-3}$ steradians). Since the angular distributions of the electrons depend on their initial kinetic energy and on the energy level from which they are ejected, this sampling of the electrons at a fixed angle will not give, in general, a true representation of the relative number of electrons within each energy group. Analyzers which collect all of the ejected electrons have been used[10] but these analyzers lack the sensitivity when radiation from a monochromator is used in contrast to the undispersed radiation from a helium discharge. This difficulty has been partially overcome by collecting the electrons ejected within a 60^{o} cone and amplifying the signal using an electron multiplier.[4] The use of a monochromator, however, introduces the additional problem of a partially polarized photon beam which varies with wavelength.[4,11] It is

the purpose of this paper to point out that a true sampling of the number of electrons within each energy group can be obtained by observing at a specific angle.

Several recent theoretical papers have dealt with the subject of the angular distributions of photoelectrons in the vacuum ultraviolet spectral range.[12-15] It has been shown that for dipole transitions the angular distribution of electrons photoejected from any energy level within an atom or molecule has the general form:

$$n \sim A + B\cos^2\alpha \qquad (2)$$

where n is the number of electrons ejected per unit solid angle by a plane polarized beam of radiation, α is the angle of ejection relative to the direction of the electric vector, while A and B are coefficients whose values depend on the energy and angular momentum of the ejected photoelectrons.

To obtain a general expression for the angular distribution when the incident radiation is partially polarized, consider the following: let a beam of partially polarized radiation be incident along the y-axis of a cartesian coordinate system (x, y, z) and let a photoelectron be ejected with direction cosines α, β, and γ as shown in Figure 11. Let I_x and I_z be the intensities of the x and z components of the incident radiation I_o, one of which lies in the main direction of polarization. Thus, $I_o = I_x + I_z$.

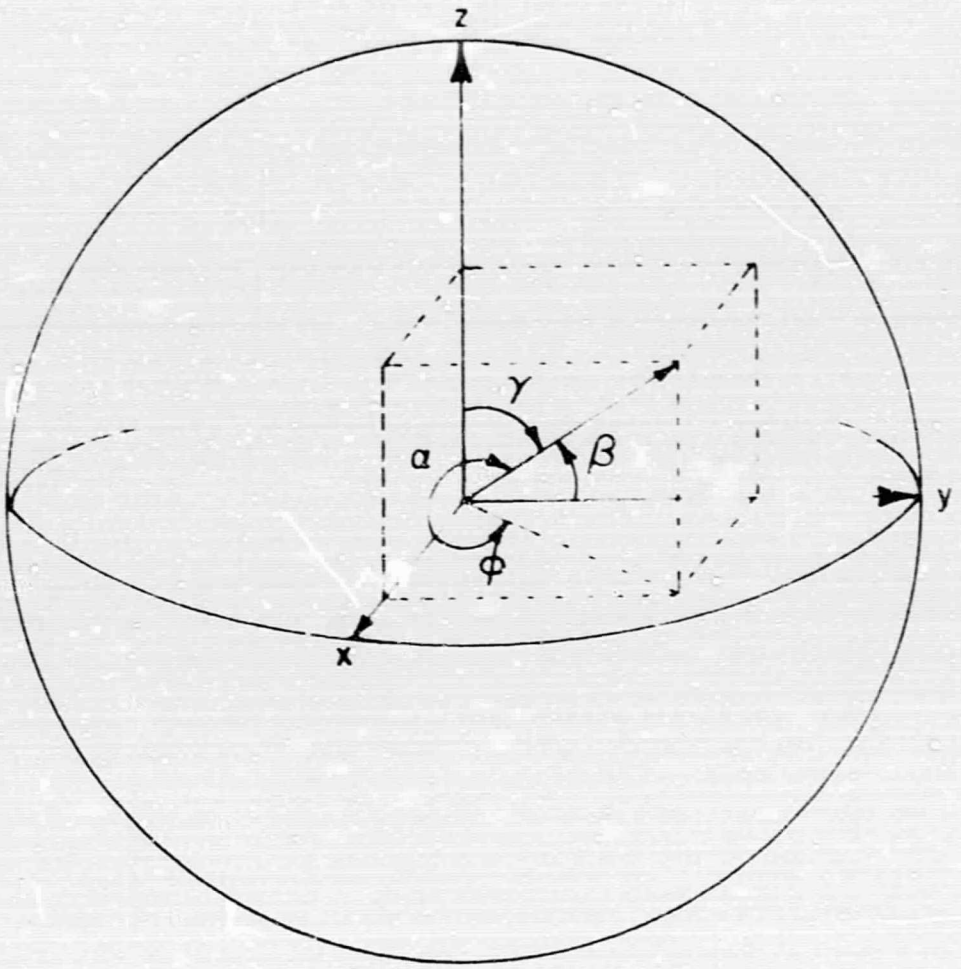

Figure 11. Angular ejection of photoelectron with respect to the x, y, and z axis. The incidence radiation is in the y-direction.

Let $$g = I_x / I_z, \tag{3}$$

then $$I_x = I_o g/(g + 1) \tag{4}$$

and $$I_z = I_o \, 1/(g + 1). \tag{5}$$

The number of electrons n ejected per unit solid angle in the direction (α, β, γ) will, therefore, be given by:

$$n = I_x \, (A + B \cos^2 \alpha) + I_z \, (A + B \cos^2 \gamma)$$

$$= I_o \, A + I_o \, B \, [g/(g + 1)] \cos^2 \alpha + I_o \, B \, [1/(g + 1)] \cos^2 \gamma,$$

$$\text{thus } n = a + b \cos^2 \alpha + c \cos^2 \gamma, \tag{6}$$

where $a = I_o A$, $b = I_o B \, g/(g + 1)$, and $c = b/g$.

g is related to the degree of polarization P by the relation $P = (g - 1)/(g + 1)$.

Equation (6) is the general expression for the angular distribution of photoelectrons ejected by partially polarized radiation. The coefficients b and c are now not only functions of the electron energy, but are also functions of the degree of polarization of the incident radiation.

The problem of obtaining a true representation of the relative number of electrons within each energy group can be solved precisely by considering Equation (6). From Equation (6), the average number of electrons, $\bar{n}$ ejected per unit solid angle can be found. By equating this value with Equation (6), the specific angles α, β, γ can be determined at which this average value can be found. Since the total number of electrons formed will always be $4\pi \, \bar{n}$, no variation in the relative numbers of the electrons will occur. The average value is given by:

$$\bar{n} = \frac{\int_0^{2\pi} (a + b\cos^2\alpha + \cos^2\gamma)\,d\omega}{\int_0^{2\pi} d\omega} \qquad (7)$$

where the incremental solid angle $d\omega = \sin\gamma \cdot d\gamma \cdot d\Phi$ and Φ is the angular direction of the photoelectrons in the x, y plane. From Figure 11, it can be shown that $\cos\alpha = \sin\gamma \cdot \cos\Phi$. Substituting the values for $\cos\alpha$ and $d\omega$ into Equation (7) and integrating we obtain

$$\bar{n} = a + b/3 + c/3 = I_o\,(A + B/3). \qquad (8)$$

Equating Equations (8) with (6), we see that the average value is obtained at angles given by $\cos^2\alpha = 1/3$ and $\cos^2\gamma = 1/3$. However, by the rule of the direction cosines, $\cos^2\alpha + \cos^2\beta + \cos^2\gamma = 1$, we obtain $\cos^2\beta = 1/3$. That is, the specific direction for which the number of electrons is equal to the average value ejected is given by

$$\alpha = \beta = \gamma = 54^o\ 44' \qquad (9)$$

Observations in this specific direction will provide the true representation of the relative numbers of electrons within each energy group regardless of the variations in the angular distribution of the photoelectrons. That is, a true representation of the relative transition probabilities will be obtained. It should be noted that the above specific angle of observation should be used in crossed beam experiments when one measures the number of electrons formed per incident photon. This ratio is proportional to the photoionization cross section of the gas involved. Also it is of interest to note that the above angle and analysis applies when measuring the cross section for Rayleigh scattering.

3. High-Resolution Quantitative Absorption Data of Minor Constituents in Planetary Atmospheres

The fact that high-resolution data are of significant importance in isolating the contribution due to minor constituents in a planetary atmosphere has been amply demonstrated in the IR spectra of planetary atmospheres. For certain specific cases, similar potential exists in the VUV region so long as the appropriate data are available. For example, it is propitious to perform measurements in those VUV spectral regions where the minor atmospheric constituent displays a cross section which far exceeds all others associated with the major constituents. These features can be even more easily isolated if the absorption features are discrete. Performance of this laboratory task is facilitated by employing a new special McPherson vacuum monochromator which GCA has recently acquired. A description of the salient features and the performance capabilities of this monochromator is included in the discussion below.

During the current quarter, the general experimental capability of obtaining VUV high resolution spectra was investigated. For these preliminary measurements, two gases were examined, namely methane and benzene. The results of these investigations are given below.

The monochromator is a McPherson model No. 225 which is a one-meter normal incidence instrument equipped with a 1200-ℓ/mm grating. The monochromator is capable of resolving 0.2Å in the first order. Attached to the exit-slit of the monochromator is a double-beam system which consists of a wedge shaped mirror oscillating a 6 cps. The radiations from

the monochromator strikes each face of the wedge at a grazing angle and is reflected into a reference and a sample cell. The surfaces of the wedge are concave which focuses the radiation into the absorption cells and prevents loss of light due to a diverging beam (see Figure 12). The cells are completely enclosed with LiF windows in front and in back of the cells. After passing through the cells, the radiation impinges onto sodium salicylate screens converting the vacuum UV radiation into near UV radiation centered around 4100Å. This radition is then detected by two matched photomultipliers. The most important and difficult problem is the matching up of the two pairs of LiF windows in both the reference and sample cells. Once this has been achieved, the log-ratio of the output signals of the two photomultipliers is proportional to the total absorption cross section of the gas in the sample cell.

The McPherson log-ratiometer is skillfully designed to allow log-ratios to be made with the many-lined spectrum of H_2. In order to facilitate the ratioing of rapidly varying intensities over several orde of magnitude in intensity, the unit first takes the signal i_r and i_f from the reference and sample-cell photomultipliers, respectively, and feeds the signals into a time sharing log-amplifier. The outputs of the log-amplifier ($\log i_r$ and $\log i_f$) are then fed into a difference amplifier giving an output

$$\log i_r - \log i_f = \log (i_r/i_f).$$

That is, the output gives the logarithm to the base ten of the ratio (i_r/i_f), (see Figure 13) which is related to the total absorption cross section as follows:

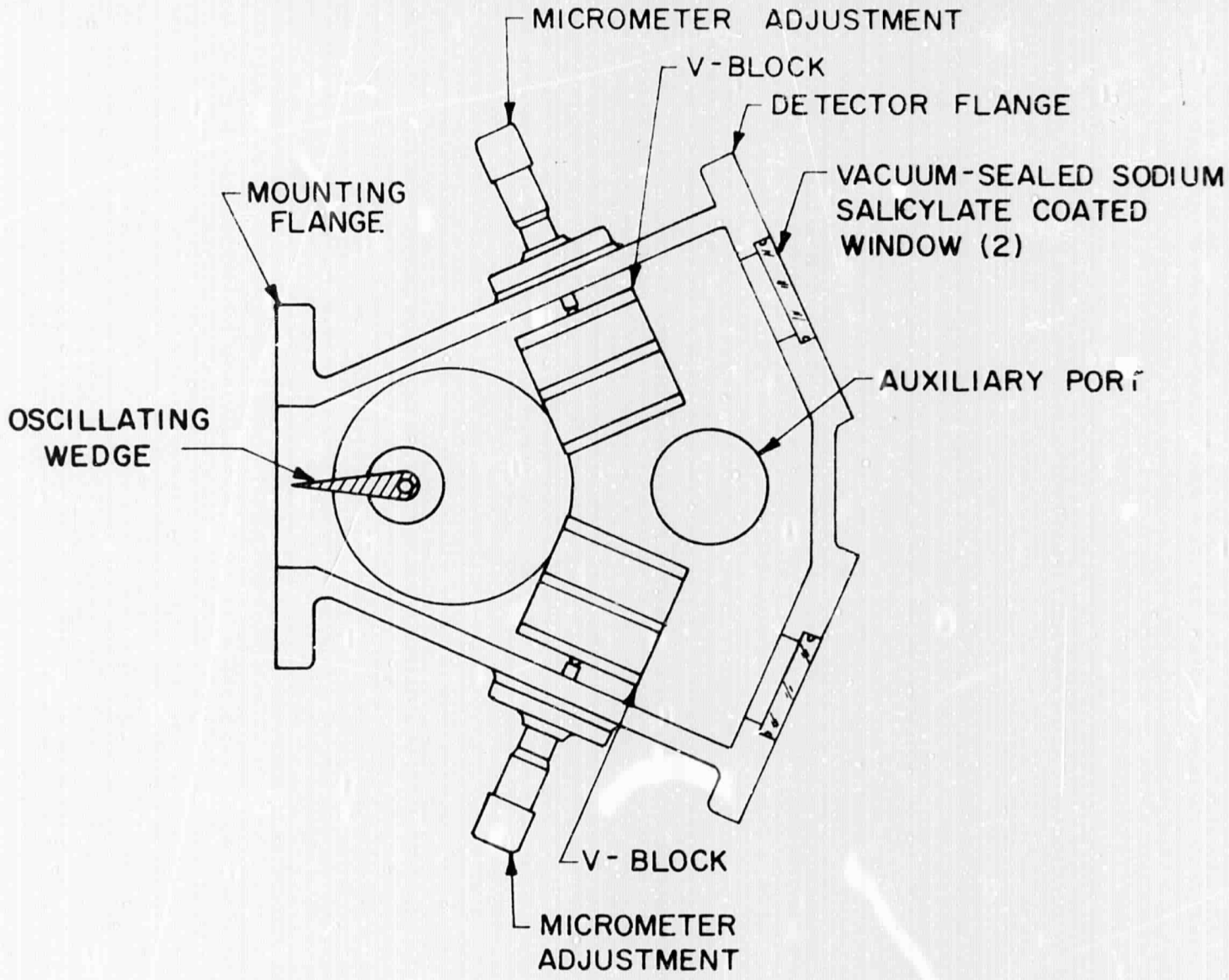

Figure 12. Diagram of double beam absorption cell housing

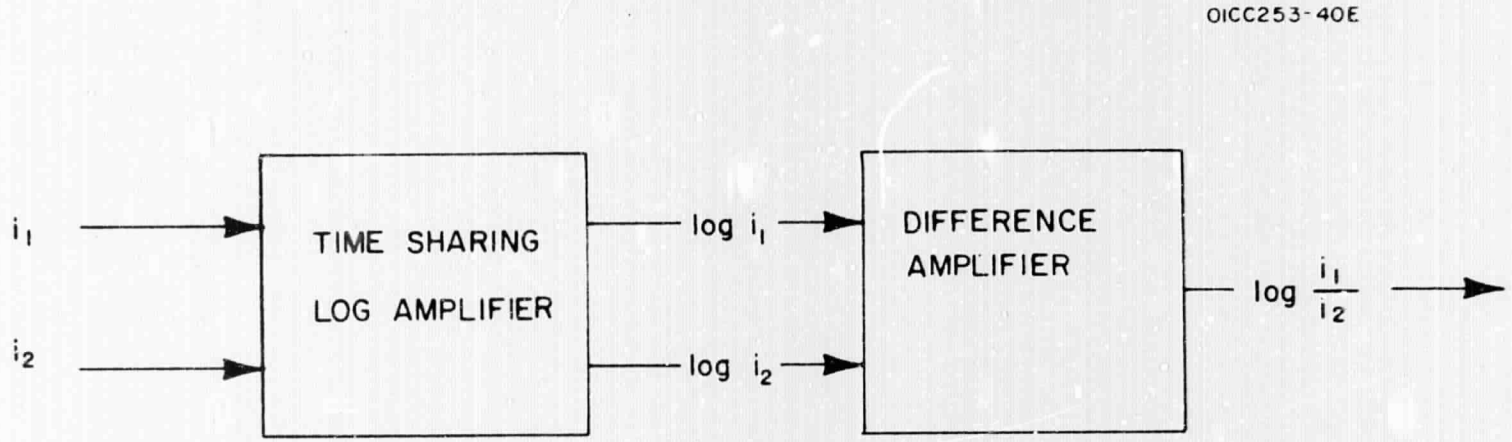

Figure 13. Block diagram of logarithmic ratiometer circuit.

$$\sigma = \frac{2.303}{nL} \log (i_r/i_f),$$

where n is the number density of the gas in the sample cell and L is the length of the sample cell.

Preliminary Results:

The total absorption cross sections of methane and benzene have been measured from 1100 to 2100Å. The results are shown in Figure 14, 15. and 16.

Methane

The only previous cross-sectional data which exists in the spectral region for methane is that of Sun and Weissler[16] and of Watanabe, et al.[17] Weissler's data has a long-wavelength limit of 1300Å and furthermore was taken at only a few points with a line spectrum. Thus, the data of Watanabe, et al. in 1953 represents the only comparable data with the presently reported results. However, their wavelength resolution was only 1Å whereas the present data was obtained with a resolution of 0.45Å. Watanabe's absolute cross sections agree with the present results over most of the wavelength region. However, the present data resolves structure below 1125Å, which they could not observe. With the exception of this structure, the absorption of methane is continuous from about 1450Å to shorter wavelengths. No absorption was observed between 1450Å and 2100Å.

Benzene:

The benzene spectrum has been studied throughly by Wilkinson[18] using photographic techniques at high resolution. However, total absorption

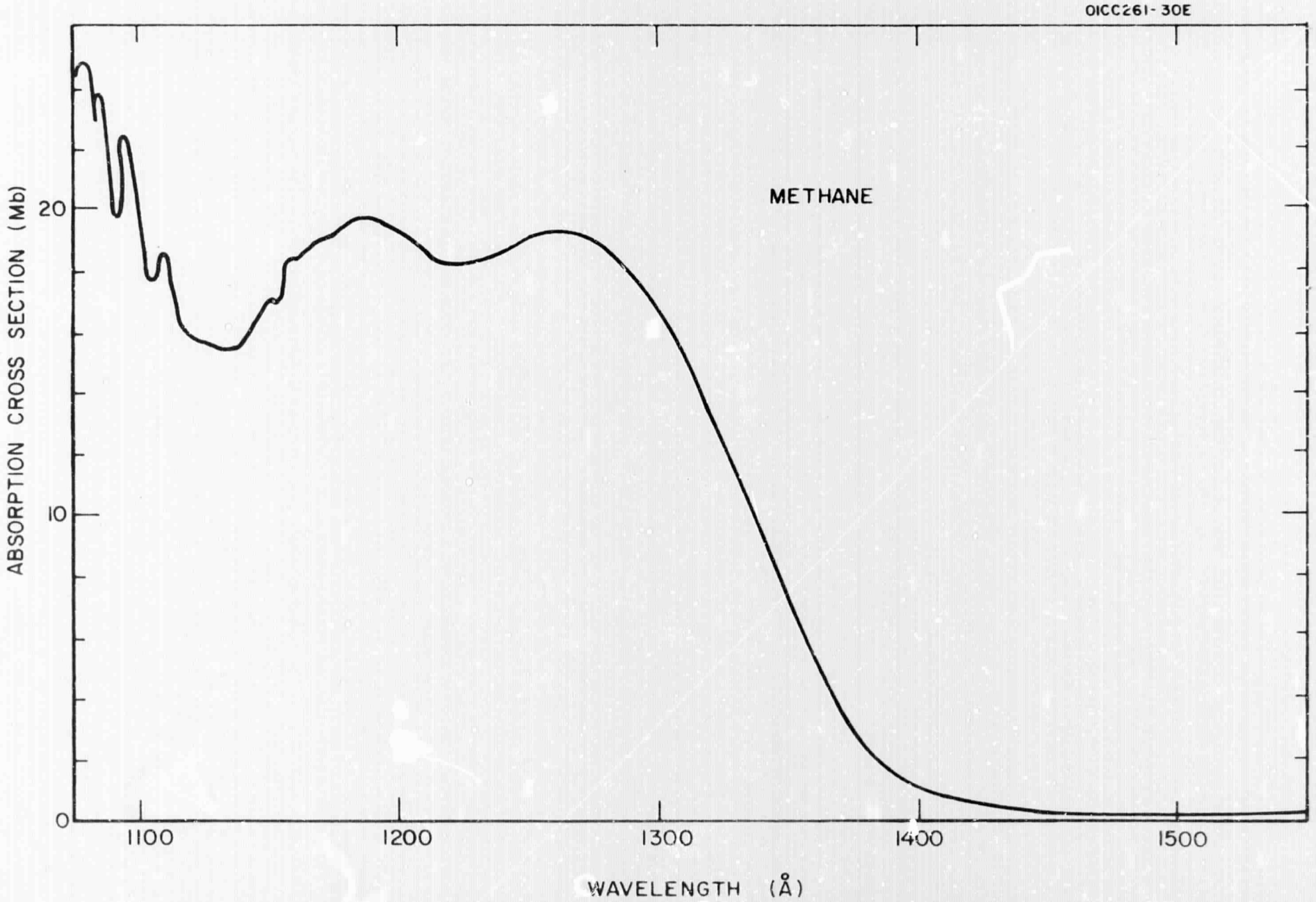

Figure 14. Absorption Spectrum of Methane between 1100 and 1500Å.

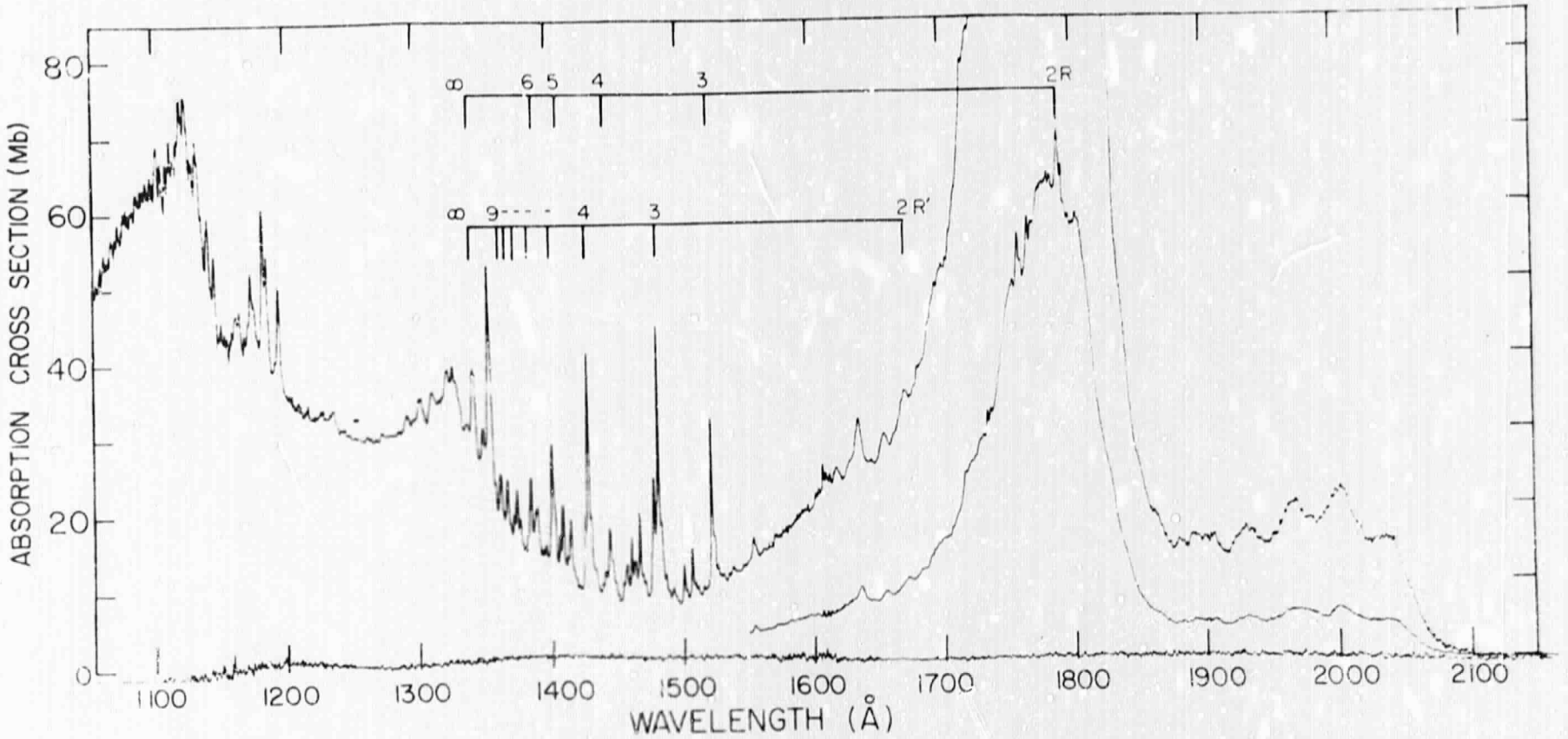

Figure 15. Absorption Spectrum of Benzene between 1100 and 2100Å.

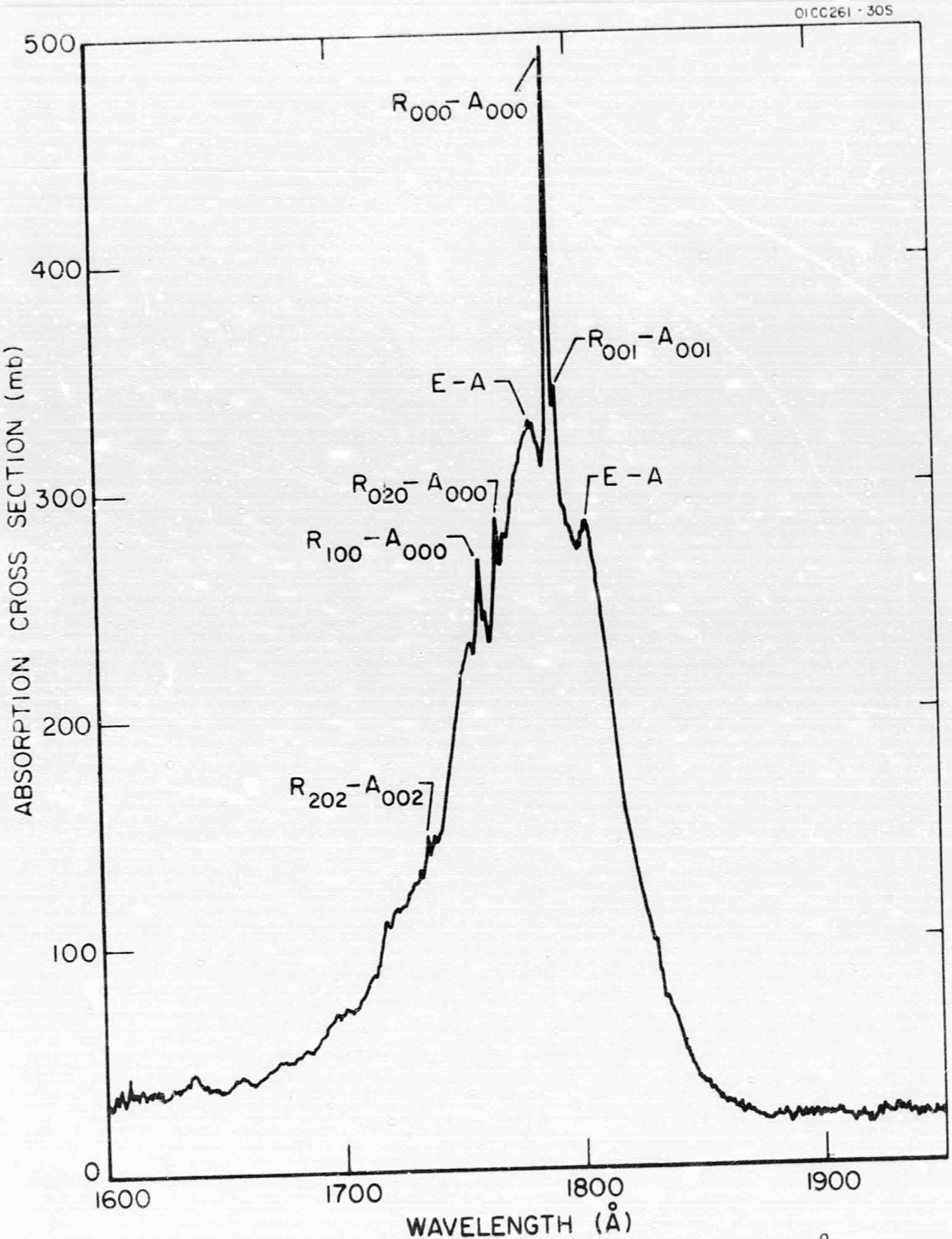

Figure 16. Absorption spectrum of Benzene between 1600 and 1900Å.

cross sections have only been made in a few isolated wavelength regions or else made at low wavelength resolution. The present data shown in Figures 15 and 16 shows considerable detailed absorption structure not readily seen with poor resolution. In Figure 15, two Rydberg series, denoted at R and R', can be seen leading up to the first ionization potential of benzene at 1340Å.

B. THEORETICAL STUDIES

In accordance with the subject work statement,it is required to perform the following theoretical studies: (1) examine the quantitative effects of electron cooling in planetary atmospheres, (2) calculate cross sections associated with ion cooling involving the fine structure bands of atomic oxygen as well as the rotational excitation of atmospheric molecules, (3) suggest, evaluate, and determine the feasibility of performing definitive experiments related to the results derived from the laboratory and theoretical studies performed under the present program requirements, (4) calculate photon scattering cross sections for $\lambda\lambda < 2500\text{Å}$, (5) evaluate the role of meteoric debris in planetary atmospheres, and (6) form calculations on the nature and intensity of VUV airglow in planetary atmospheres owing to EUV-produced photoelectrons.

During the current reporting period,effort has been directed toward completing task items 1, 2 and 3. Items 1 and 2 have now been completed and are reported below. Concerning item #3, only preliminary considerations have been developed, but these are also included in this report in some detail for future reference.

1. Effect of Oxygen Cooling on Ionospheric Electron Temperatures.

The results of this investigation are contained below. The detailed results are available in a paper entitled "The Effect of Oxygen Cooling on Ionospheric Electron Temperatures" by A. Dalgarno, et al. which has been recently submitted for publications to Planetary and Space Sciences.

It has been pointed out recently[19] that excitation of the fine-structure levels of atomic oxygen by electron impact contributes substantially to the cooling of the electron gas in the ionosphere of the Earth. Its inclusion in the description of the thermal balance may resolve the discrepancies that exist between theoretical predictions of electron temperatures in the F-region[7] and values derived from Thompson scatter data.[20-27]

The calculation of the altitude profile of the heating rates of electron gas resulting from the absorption of solar electromagnetic radiation in the atmosphere has been described in detail.[8,28] We have employed the same atmospheres and ionospheres (with the addition of an atomic hydrogen component)[29] and the same solar fluxes[7,30] described. We have modified the earlier calculations by the substitution of improved data on the photoionization of atomic oxygen. The photoionization cross section is a composite of the background and resonance contributions that arise from autoionizing transitions. We adopted for the background contributions, the total cross sections calculated,[31] which are in agreement with the experimental data of Comes, Speier and Elzer;[32] for the resonance contributions, we adopted values consistent with the experimental data of Cairns and Samson.[33] A detailed tabulation has been presented by Henry and McElroy.[34] For the relative cross sections of photoionizing transitions terminating in the ^4S, ^2D, and ^2P states of O^+, we adopted branching ratios obtained by averaging the calculations of Henry[35] over wavelength.

It was noted earlier[28] that uncertainties exist in the derived heat fluxes because of the possibility that vibrationally excited nitrogen, produced by photoelectron impact, might be deactivated by superelastic collisions with the ambient thermal electrons. Because of diffusion and neutral-particle deactivation, it seems unlikely that vibrationally excited nitrogen is a significant hear source for the electron gas, so we have not included it. We have confirmed that the contributions from the deactivation of the metastable ionic states by thermal electron impact is negligible. In the F-region, the metastable ions are removed by ion-molecule reactions. At higher altitudes, some contribution to electron heating occurs, but its magnitude is much less than are the uncertainties arising from the imprecision of the basic photoabsorption cross sections, from the description of the energy degradation of the photoelectrons as a continuous energy-loss process,[36] and from the assumption that the photoelectron energy is deposited locally.[37-40]

Hanson and Johnson[41] introduced a photoelectron heating-efficiency parameter ϵ, defined as the quotient of Q eV cm^{-3} sec^{-1} and the electron production rate η cm^{-3} sec^{-1}. Our predicted values of ϵ in the eV are illustrated in Figures 17 and 18. Figure 17 shows that, except early in the day when the ambient electron density is increasing rapidly, the value of ϵ at any given altitude is nearly constant.

In an atmosphere in which the relative neutral-particle composition is not changing with altitude, the photoelectron heating-efficiency parameter ϵ increases steadily with increasing altitude toward

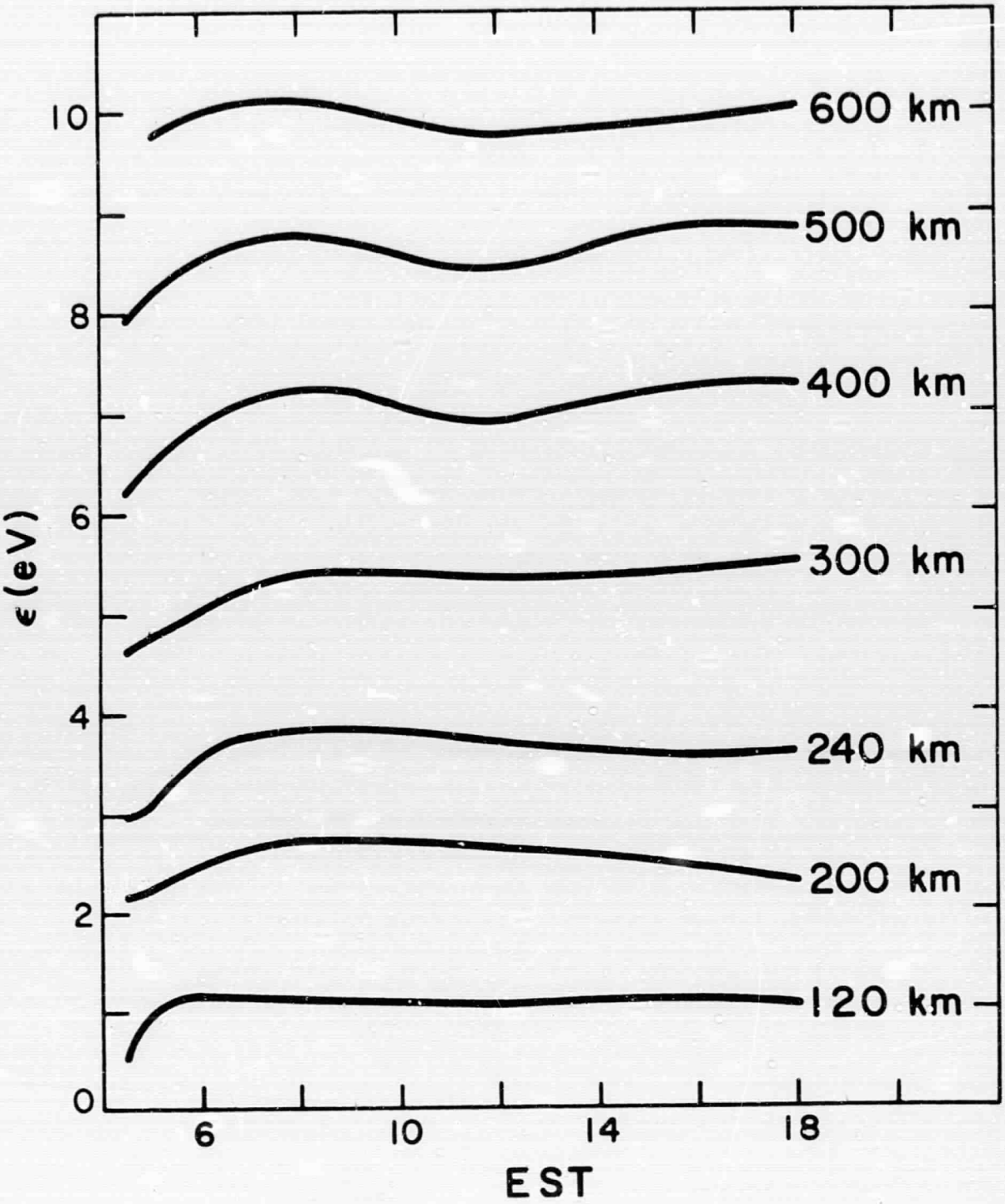

Figure 17. Mean electron heating per ionization, ϵ(eV), at selected altitudes throughout the day.

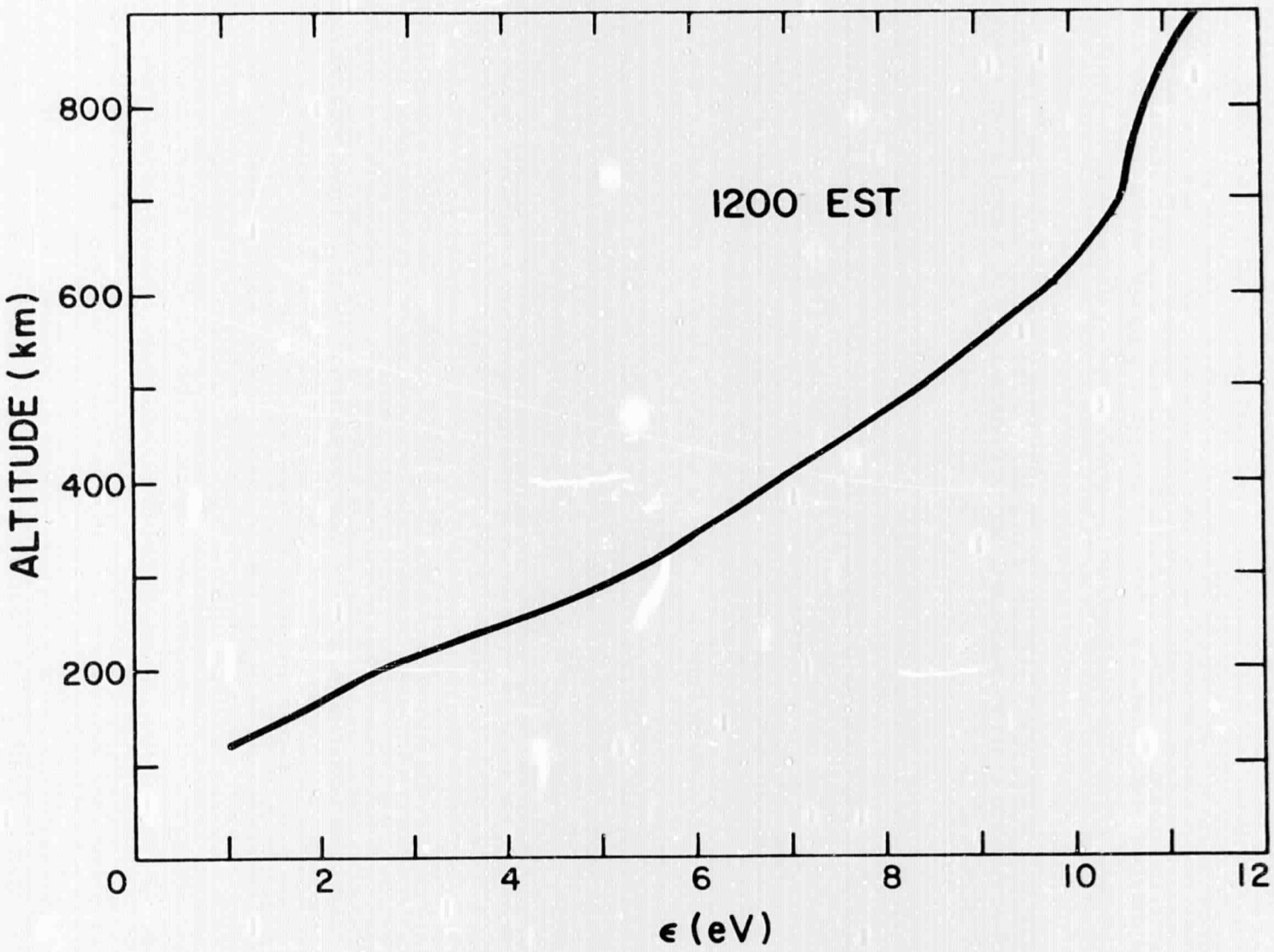

Figure 18. The altitude profile of the mean electron heating per ionization at noon.

a constant limiting value. The behavior of ϵ in the actual atmosphere is slightly more complicated because ϵ tends initially to a value of about 10 eV controlled by the absorption by atomic oxygen and then with increasing altitude to a value of about 12 eV controlled by the absorption by helium. Ultimately, it will tend to a limiting value controlled by the absorption of hydrogen. The change from oxygen to helium is reflected in the altitude profile, shown in Figure 18. At high altitudes, the values of ϵ appropriate to the atmosphere will be augmented by contributions to Q from the non-local escaping photoelectrons.

Hanson and Cohen[40] have recently derived empirical values of ϵ from measurements of the electron density n_e and the electron temperature T_e at Jicamarca. At altitudes near 300 km, their derived values are somewhat larger than are the values in Figures 17 and 18. The comparison indicates that Hanson and Cohen may have underestimated the electron-production rates. At low altitudes there is a serious descrepancy, the empirical estimates being much smaller than the theoretical values. Indeed, Hanson and Cohen conclude that if the electron-production rates are not considerably smaller than they have calculated, either the measurements of T_e are seriously in error or some efficient energy-loss process between electrons and neutral particles has been overlooked. The electron-production rates derived by Hanson and Cohen are, in fact, comparible to those predicted by studies of the absorption of solar ionizing radiation[28,42] and we suggest that the discrepancy can be largely attributed to the omission of the cooling that arises from the excitation of the fine-structure levels of atomic oxygen.

The heated electron gas cools through a number of different mechanisms. The rate at which the electron gas loses heat to a positive ion mixture of O^+, NO^+, O_2^+, He^+, and H^+ is given approximately by[43]

$$L_e = \frac{5 \times 10^{-7} (T_e - T_i)}{T_e^{3/2}} n_e \left[n(O^+) + 0.53\, n(NO^+) + 0.50\, n(O_2^+) + 4\, n(He^+) + 16\, n(H^+) \right] \text{ eV cm}^{-3} \text{ sec}^{-1},$$

where $n(X^+)$ is the appropriate ion density and T_i is the ion temperature. In practice, the different positive ions have different temperatures at high altitudes,[8,44] but the effect on the electron temperature is negligible. The adopted ion distribution is based upon the mass-spectrometric measurements by Holmes, Johnson and Young.[45-47]

Previous work has included the contributions to cooling from elastic collisions with the neutral particles, from rotational and vibrational excitation of N_2 and O_2, and from excitation of O to the ^1D level. For the contribution from elastic collisions, we have used the expressions listed by Banks;[48] for rotational excitation of N_2 we have employed the formula of Dalgarno and Henry;[49] and for rotational excitation of O_2, we have used the expression:

$$\frac{dU_e}{dt} = -n_e\, n(O_2)\, 7 \times 10^{-14} \frac{(T_e - T_n)}{T_e^{1/2}} \text{ eV cm}^{-3} \text{ sec}^{-1},$$

where T_n is the neutral-particle temperature and $n(O_2)$ is the number density of O_2. The expression follows from substitution of the empirical quadrupole moment of O_2 derived by Hake and Phelps[50] into the formula of Mentzoni and Row.[51] The cooling rate from vibrational excitation

of N_2 was calculated following the procedures described by Rees, Walker and Dalgarno,[52] and it is shown in Figure 19 for various values of the neutral-particle temperature. We have not considered cooling arising from vibrational excitation of O_2 nor that arising from excitation to the a $^1\Delta_g$ and b $^1\Sigma_g^+$ electronic states of O_2. The cooling due to collisions with O_2 is not significant in the F-region of the ionosphere.

We have included the previously neglected contribution from the fine-structure excitation process

$$e + O(^3P_J) \rightarrow e + O(^3P_{J'}),$$

the efficiency of which has been calculated by Dalgarno and Degges.[19] Figure 20 is a comparison of the contributions from the individual processes for the 1200 EST electron-temperature distribution tabulated in the appendix. It is clear that fine-structure excitation is the dominant process throughout the E- and F-regions of the ionosphere.

In order to calculate the electron temperatures, we must also take account of ion cooling. For the energy transfer of ions moving in their parent gases we have adopted the expressions listed by Banks,[53] and for the energy transfer of ions moving in unlike gases we have adopted a mean momentum transfer cross section of 8×10^{-15} cm^2.[54]

The method of solution of the equations describing the thermal balance of the electron and ion gases, which include the influence of thermal conduction in the electron gas, has been described by Walker and Rees,[55] where an expression is given for the coefficient of thermal conductivity

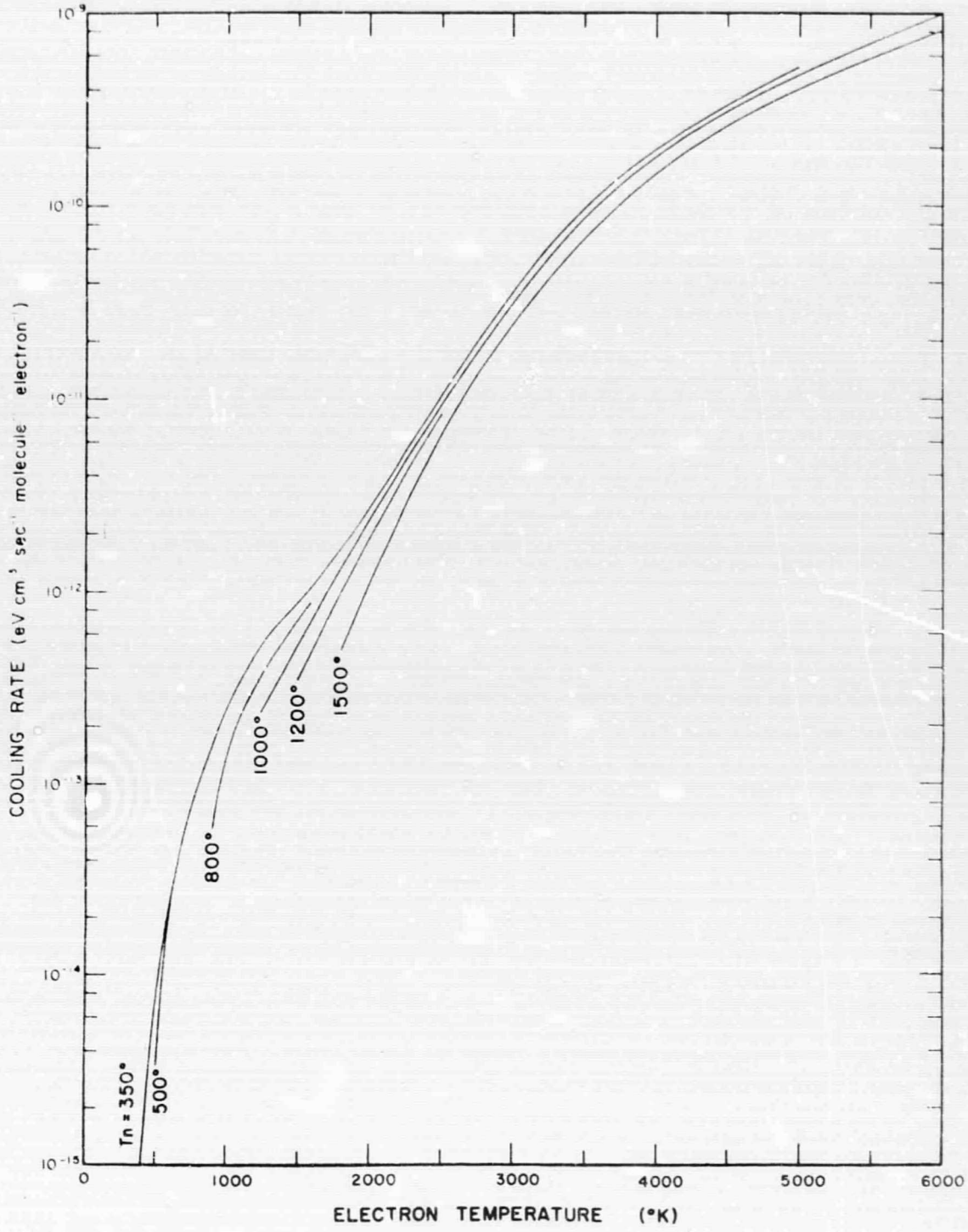

Figure 19. The electron cooling rates per electron per molecule from excitation of vibrational levels in molecular nitrogen. The rates depend both on electron temperature T_e and on the neutral-particle temperature T_n.

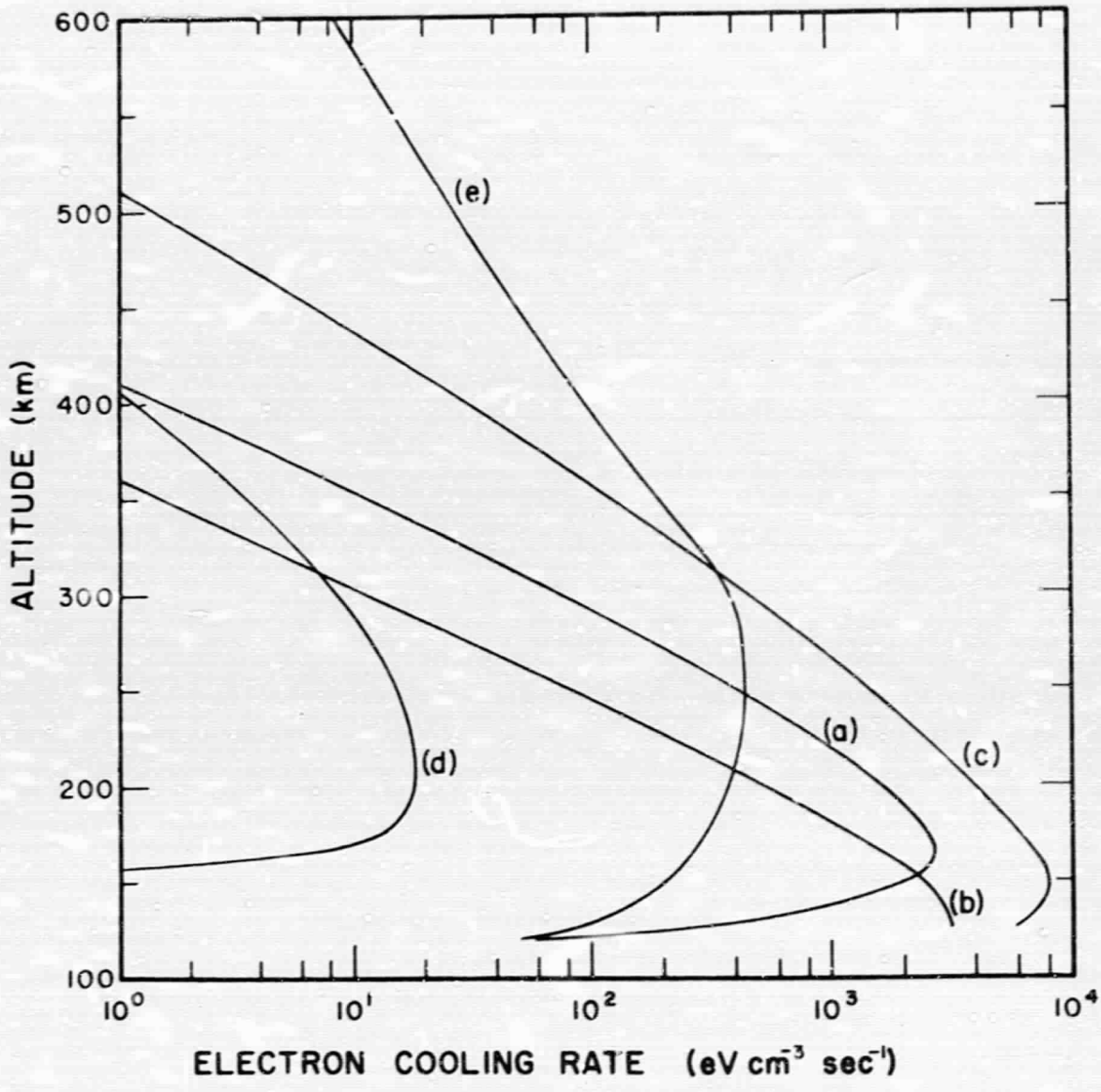

Figure 20. The electron cooling rates appropriate to the atmosphere and ionosphere at noon, July 1963. The curves show cooling resulting from excitation of (a) vibrational levels of molecular nitrogen, (b) rotational levels of molecular nitrogen, (c) fine-structure levels of atomic oxygen, (d) metastable levels of atomic oxygen, and (e) elastic collisions with positive ions. The rates from elastic collisions with neutral particles and from rotational excitation of molecular oxygen are negligibly small.

appropriate to the ionosphere. We have not included the effect of ionic conductivity: It appears from the calculations of Banks[56,57] that the effect of ionic conductivity is not important below 700 km.

We have selected for comparison the Thomson scatter data of Evans[20] for the month of July, 1963, since the solar flux data of Hinteregger, et al.[30] that we have used are strongly weighted by measurements made during July, 1963. The observations for July, 1963 indicate an essentially isothermal regime at great altitudes, and our comparison is not complicated by the possible existence of a substantial heat flux from above. The use of a small conductive flux of 2.46×10^9 eV cm^{-2} sec^{-1} as a boundary condition in the solution of the thermal balance equation for noon in July, 1963 altered the temperature at 600 km from 2565°K to 2618°K and at 500 km from 2535°K to 2539°K; the temperatures below 500 km remained unchanged. Figures 21 and 22 correspond to a vanishing conductive flux at 600 km.

The electron temperatures predicted for various times throughout the day with allowance for the effect of cooling due to fine structure are compared in Figure 21 with the earlier calculations that omitted the oxygen cooling mechanism. The cooling due to fine-structure excitation effects substantial reductions in the predicted electron temperatures and brings the predicted electron temperature into remarkably close agreement with the values measured above 320 km. The closeness of the agreement at these heights is emphasized in Figure 22 which compares the predicted diurnal variations at several altitudes with the observed diurnal variations. The present heating rates are somewhat larger than are the earlier values,

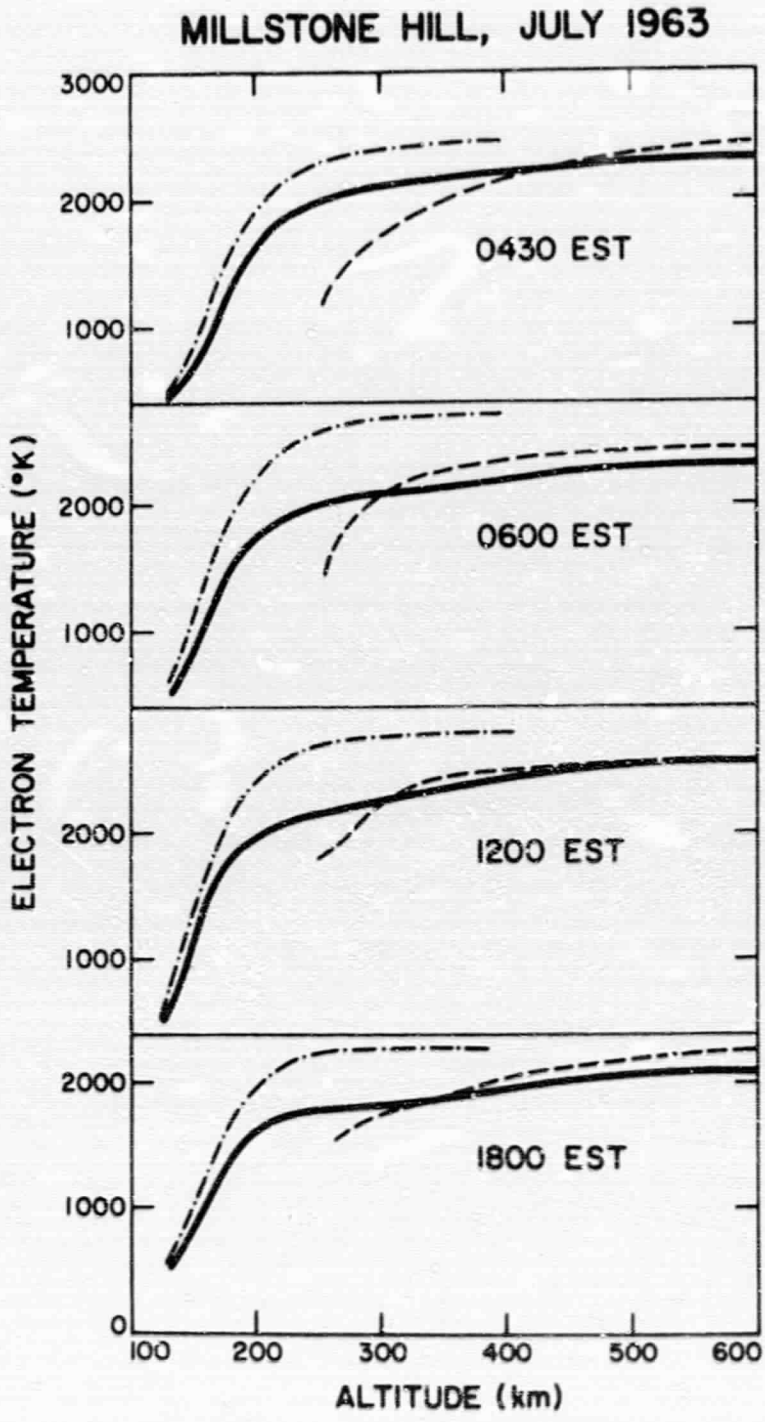

Figure 21. Electron-temperature/height profiles in July 1963 at various times throughout the day. The dash-hot curves exclude electron cooling to atomic oxygen; the solid curves include it; the dashed curves are the data of Evans (1965).

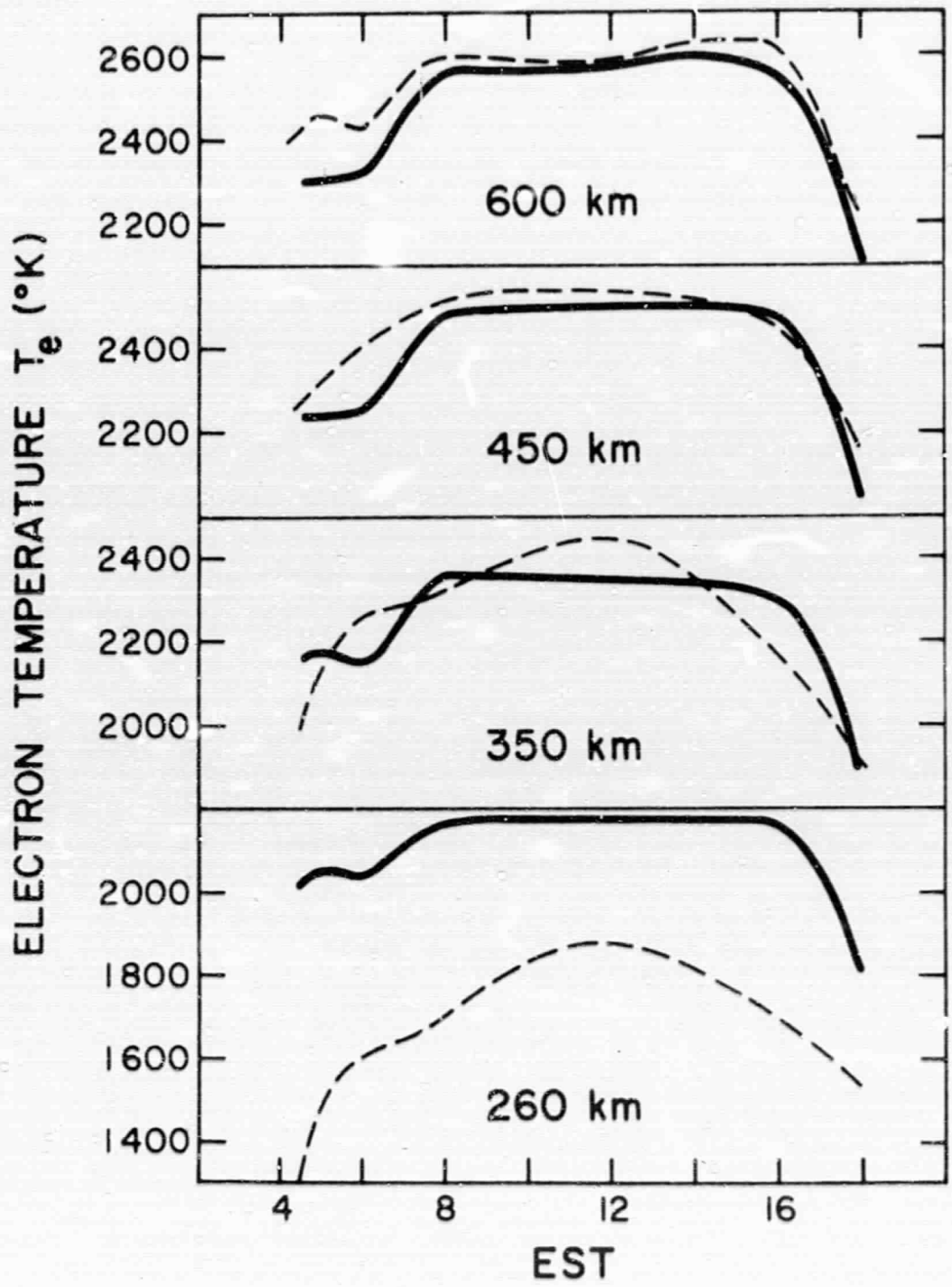

Figure 22. Comparison of the calculated (solid line) and measured (dashed line) diurnal variations of electron temperatures at selected altitudes.

so that the effect of oxygen cooling is actually greater than that suggested by the figures.

The discrepancy at altitudes below 300 km, noted previously,[8] is maintained. However, with the inclusion of the fine-structure cooling process, we can obtain agreement with observation by arbitrarily reducing the heat input at 250 km by about 30% and at 200 km by about 60%.

The uncertainties in the calculated heat- input profile are large, but the detailed agreement obtained at high altitudes suggests that the main features of the thermal balance are correctly described. The predicted heat input between 120 and 300 km could be decreased by modifications in the photoionization and photoabsorption cross sections at shorter wavelengths (such as a reduction in the fraction of the total absorption that results in electron-ion production). The predicted heat input could also be decreased below 300 km by a decrease in the adopted solar flux at shorter wavelengths or by the postulation of a highly efficient energy-loss mechanism for photoelectrons in molecular oxygen. The last possibility, which would also enhance the cooling rate, is not supported by the cross section analysis of Hake and Phelps.[50]

TABLE 1

Measured electron densities (n_e) and computed electron heating rates (Q), electron temperatures (T_e), and electron production rates (η) for July 1963 at Millstone Hill; EST is Eastern Standard Time, T_∞ is the neutral temperature in the exosphere, and θ is the solar zenith angle.

Z	n_e	Q	T_e	η	n_e	Q	T_e	η
(km)	(cm^{-3})	(eV cm^{-3} sec^{-1})	(°K)	(electrons cm^{-3} sec^{-1})	(cm^{-3})	(eV cm^{-3} sec^{-1})	(°K)	(electrons cm^{-3} sec^{-1})
	0430 EST; T_∞ = 716°K; θ = 87.6°				0600 EST; T_∞ = 734°K; θ = 72.1°			
120	2.4(4)*	6.95(1)	357	1.24(2)	7.0(4)	1.67(3)	-	1.44(3)
140	4.0(4)	3.18(2)	549	1.98(2)	9.0(4)	3.07(3)	662	2.20(3)
160	5.4(4)	5.12(2)	841	3.06(2)	1.2(5)	4.21(3)	1090	2.49(3)
180	6.8(4)	9.08(2)	1300	4.75(2)	1.6(5)	4.74(3)	1500	2.27(3)
200	8.3(4)	1.20(3)	1630	5.57(2)	1.8(5)	4.31(3)	1750	1.72(3)
220	9.4(4)	1.37(3)	1820	5.42(2)	1.9(5)	3.34(3)	1890	1.12(3)
240	9.5(4)	1.30(3)	1940	4.35(2)	1.9(5)	2.45(3)	1970	6.84(2)
260	9.0(4)	1.07(3)	2010	3.04(2)	1.7(5)	1.68(3)	2020	4.08(2)
280	8.5(4)	8.19(2)	2060	1.98(2)	1.5(5)	1.12(3)	2060	2.44(2)
300	7.7(4)	5.75(2)	2100	1.24(2)	1.3(5)	7.38(2)	2090	1.47(2)
320	6.7(4)	3.90(2)	2120	7.74(1)	1.1(5)	4.83(2)	2110	8.93(1)
340	5.7(4)	2.60(2)	2140	4.80(1)	1.0(5)	3.19(2)	2130	5.49(1)
360	4.8(4)	1.71(2)	2160	2.98(1)	8.8(4)	2.11(2)	2150	3.41(1)
380	3.8(4)	1.12(2)	2180	1.86(1)	7.9(4)	1.40(2)	2170	2.13(1)
400	2.9(4)	7.24(1)	2200	1.17(1)	6.6(4)	9.21(1)	2200	1.35(1)
500	1.5(4)	1.00(1)	2270	1.26	3.4(4)	1.29(1)	2290	1.51
600	8.0(3)	1.89	2300	1.94(-1)	1.7(4)	2.32	2320	2.31(-1)
	0800 EST; T_∞ = 766°K; θ = 50.2°				1200 EST; T_∞ = 809°K; θ = 21.5°			
120	1.2(5)	5.29(3)	-	4.76(3)	1.3(5)	9.40(3)	404	9.17(3)
140	1.5(5)	8.20(3)	764	5.87(3)	1.7(5)	1.23(4)	869	8.70(3)
160	1.8(5)	9.20(3)	1270	5.05(3)	1.9(5)	1.25(4)	1450	6.70(3)
180	2.2(5)	8.31(3)	1640	3.72(3)	2.1(5)	1.00(4)	1810	4.49(3)
200	2.6(5)	6.34(3)	1840	2.36(3)	2.4(5)	7.15(3)	1970	2.72(3)
220	2.7(5)	4.46(3)	1970	1.39(3)	2.6(5)	4.93(3)	2060	1.60(3)
240	2.8(5)	3.12(3)	2070	8.13(2)	2.7(5)	3.45(3)	2120	9.35(2)
260	2.7(5)	2.11(3)	2160	4.77(2)	2.8(5)	2.40(3)	2170	5.56(2)
280	2.5(5)	1.40(3)	2240	2.84(2)	2.6(5)	1.61(3)	2210	3.37(2)
300	2.2(5)	9.25(2)	2280	1.72(2)	2.4(5)	1.09(3)	2250	2.07(2)
320	2.0(5)	6.13(2)	2310	1.06(2)	2.2(5)	7.36(2)	2290	1.30(2)
340	1.7(5)	4.04(2)	2350	6.60(1)	2.0(5)	4.98(2)	2330	8.24(1)
360	1.5(5)	2.69(2)	2380	4.16(1)	1.7(5)	3.36(2)	2370	5.29(1)
380	1.3(5)	1.80(2)	2410	2.64(1)	1.4(5)	2.27(2)	2400	3.43(1)
400	1.2(5)	1.22(2)	2440	1.69(1)	1.2(5)	1.55(2)	2430	2.24(1)
500	6.2(4)	1.79(1)	2530	2.04	6.5(4)	2.50(1)	2540	2.96
600	3.2(4)	3.19	2560	3.16(-1)	3.6(4)	4.65	2570	4.76(-1)
	1600 EST; T_∞ = 829°K; θ = 57.4°				1800 EST; T_∞ = 811°K; θ = 79.1°			
120	9.1(4)	3.83(3)	-	3.49(3)	4.9(4)	7.99(2)	366	7.77(2)
140	1.1(5)	6.02(3)	809	4.45(3)	6.2(4)	1.36(3)	657	9.46(2)
160	1.3(5)	6.85(3)	1370	4.03(3)	8.4(4)	2.11(3)	1040	1.29(3)
180	1.5(5)	6.74(3)	1800	3.27(3)	1.1(5)	2.62(3)	1410	1.37(3)
200	1.7(5)	5.57(3)	2000	2.30(3)	1.4(5)	2.89(3)	1630	1.27(3)
220	2.0(5)	4.24(3)	2090	1.48(3)	2.0(5)	2.86(3)	1730	1.01(3)
240	2.5(5)	3.28(3)	2130	9.20(2)	2.5(5)	2.57(3)	1780	7.15(2)
260	2.9(5)	2.43(3)	2160	5.68(2)	3.0(5)	2.07(3)	1800	4.75(2)
280	3.1(5)	1.72(3)	2190	3.52(2)	3.2(5)	1.53(3)	1820	3.07(2)
300	3.1(5)	1.19(3)	2220	2.21(2)	3.2(5)	1.08(3)	1830	1.96(2)
320	2.9(5)	8.17(2)	2250	1.40(2)	3.0(5)	7.49(2)	1850	1.26(2)
340	2.7(5)	5.61(2)	2290	9.01(1)	2.8(5)	5.15(2)	1880	8.11(1)
360	2.5(5)	3.86(2)	2330	5.85(1)	2.4(5)	3.51(2)	1910	5.26(1)
380	2.2(5)	2.65(2)	2370	3.83(1)	2.0(5)	2.38(2)	1940	3.43(1)
400	2.0(5)	1.84(2)	2400	2.53(1)	1.8(5)	1.64(2)	1970	2.25(1)
500	1.1(5)	3.05(1)	2520	3.48	1.0(5)	2.65(1)	2090	3.00
600	6.2(4)	5.70	2560	5.72(-1)	5.6(4)	4.87	2130	4.85(-1)

*2.4(4) ≡ 2.4×10^4

2. Mars Lander Experiment -- Spectral Photometric Observations of the Martian Atmospheric Dayglow.

The identification of the atomic and molecular constituents in a planetary atmosphere is a fundamental branch of planetary aeronomy. For the Earth atmosphere, one of the most prolific sources for these type of data have been obtained through the performance of airglow observations employing ground based spectro-photometric techniques. However, the performance of such experiments are severely constrained owing to two important limitations: (a) the spectral region of investigation is limited to wavelengths greater than 3000Å owing to atmospheric attenuation, and (b) throughout the visible regions intense background radiations (on the order of megarayleighs) can be encountered owing to Rayleigh and Mie scattering of the solar illuminated atmosphere.

On the other hand, owing to the relatively tenuous and transparent (down to 2000Å) atmosphere which surrounds the planet Mars, the above cited constraints are significantly minimized. For example, it can be shown that the background intensities encountered throughout the feasible region are about two orders of magnitude less than those encountered on the surface of the Earth. (This condition obtains for a platform situated 30 km above the Earth's surface.) Furthermore, on Mars, ground-based airglow observations can be performed at wavelengths as short as 2000Å.

To evaluate the feasibility and potential involved in the performance of a Mars Lander airglow experiment, a number of initial tasks were performed during the current quarter; those are described below.

a. Calculated Estimates of the Rayleigh Scattering Background Radiation for Dayglow Observation.

To calculate the dayglow background intensities due to Rayleigh scattering from the solar illuminated Martian atmosphere, the following pertinent parameters are involved: (1) a suitable model for the major constituency and altitude profiles for the lower atmosphere of Mars, (2) the incident solar flux, (3) the pertinent absorption and Rayleigh scattering cross sections σ_a and σ_s respectively for the major atmospheric constituents, and finally (4) the availability of a suitable theoretical relationship in order to perform the required calculations.

The model atmosphere employed in the present study is shown in Figure 23 where the number densities are given as a function of altitude for a completely mixed CO_2 - N_2 Martian atmosphere. The selected composition of 64% CO_2 and 36% N_2 by volume and the total surface pressure of 7 mbars was derived on the basis of Mariner IV experimental data.[58] The model should be especially accurate so far as the lower atmosphere is concerned; in the present case, this is fortunate since the calculated background radiations are essentially established by this region of the atmosphere. An estimate for the incident mean solar flux was obtained by applying a scaling factor of 0.43 to previously published incident flux for Earth.[59] Concerning the absorption and scattering cross sections for CO_2 and N_2, the following comments apply. First, it should be noted that both of these gases are essentially transparent toward absorption for $\lambda\lambda$ 2000 - 8000Å. Accordingly for this wavelength region, atmospheric attenuation of the incident solar flux is due primarily to scattering by N_2 and

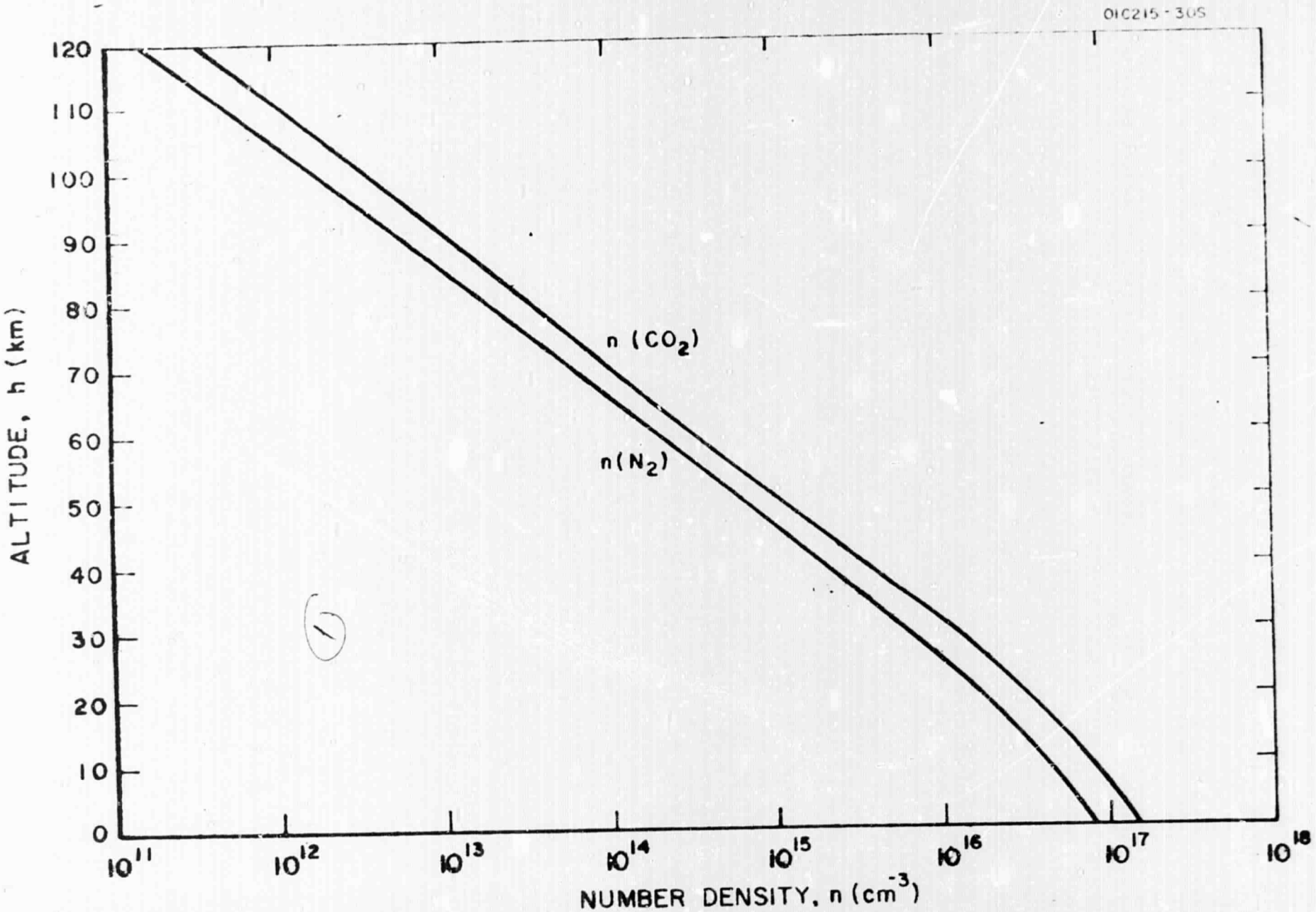

Figure 23. Number densities as a function of altitude in the Martian Atmosphere of CO_2 and N_2 for the selected model.

CO_2. Figure 24 shows the Rayleigh scattering cross sections for N_2 and CO_2 as a function of wavelength for λλ 2000 - 8000Å. The σ_s (N_2)-values were taken directly from a recent report by A. Dalgarno, et al[60] whereas the corresponding $\sigma_s(CO_2)$ values were calculated on the basis of the following formula.

$$\sigma_s(CO_2) = \frac{8\pi^3 [n^2(\lambda) - 1]^2}{3 N^2 \lambda^4} \quad \frac{6 + 3\rho}{6 - 7\rho} \tag{10}$$

where $n(\lambda)$ = refractive index

N = Loschmidt's number = 2.7×10^{19} cm^{-3}

ρ = deplorization factor.

The refractive index data were obtained directly from the literature[61] and a ρ value of 0.098[61] was applied throughout the entire spectral region of interest.

For the atmospheric model and σ_s- values employed, it can be shown that the Martian atmosphere is essentially transparent to radiation for wavelengths down to 2000Å. This conclusion is in accord with the experimental data due to Evans.[62]

Employing the parameters above the intensity of the Rayleigh scattering, background from the solar illuminated Martian atmosphere was calculated from the following equation.

$$S(\lambda,x,h) = P(x)\ \Phi\ (\lambda) \sum_i \sigma_i\ (\lambda)\ N_i\ (h) \tag{11}$$

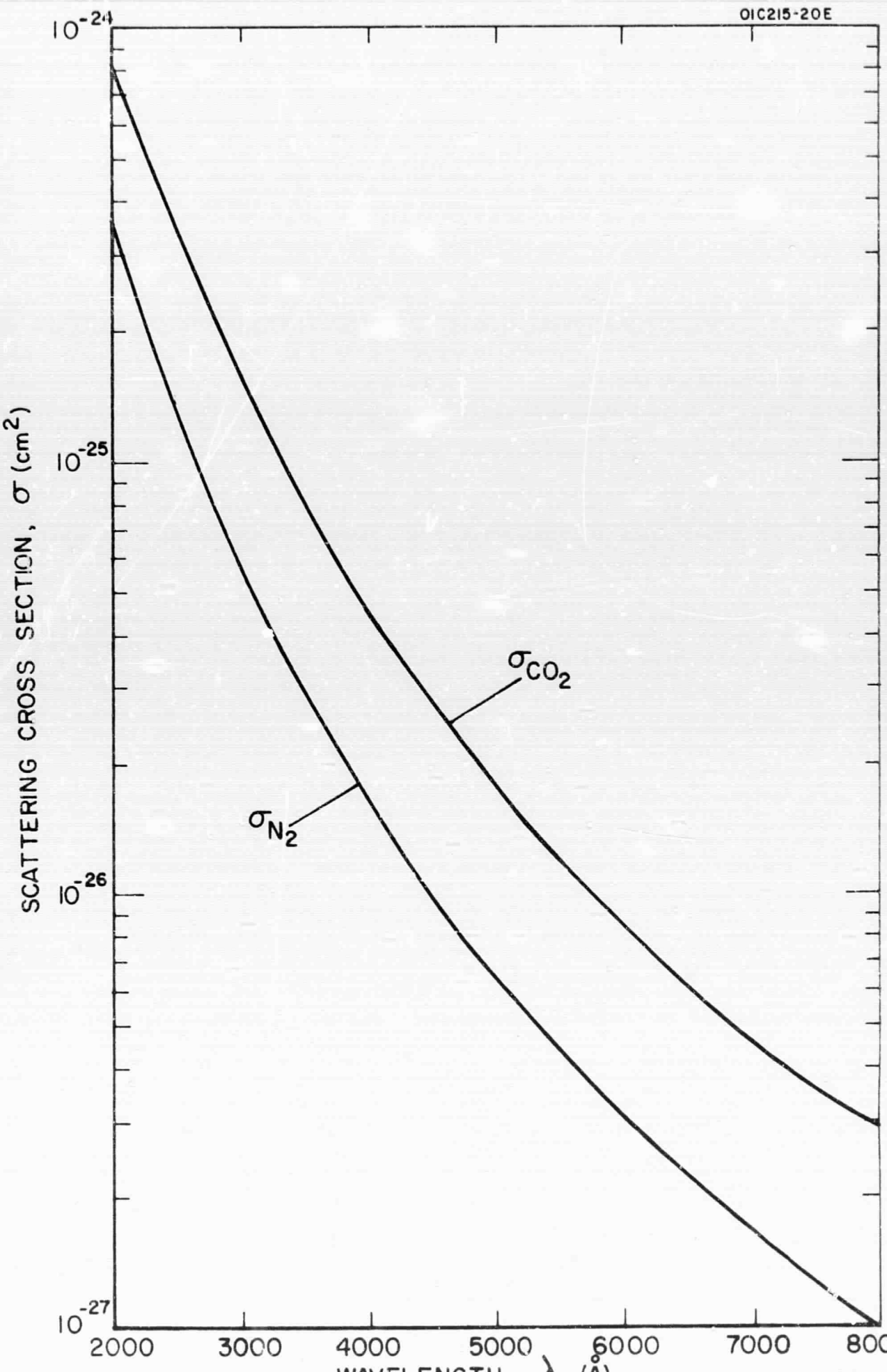

Figure 24. Rayleigh Scattering Cross Sections of CO_2 and N_2 as a function of wavelength.

where:

$S(\lambda,x,h)$ = Rayleigh scattering background level (Photons/cm^2 sec Å)

$\Phi(\lambda)$ = solar flux (photons/cm^2 sec Å)

$P(x)$ = Rayleigh scattering phase function $3/4\ (1 + \cos^2 x)$

x = scattering angle

σ_s = Rayleigh scattering cross-section of the i^{th} constituent (cm^2)

N_i = column count of the i^{th} constituent (cm^{-2})

The present estimates pertain to the zenith sky radiance for a solar zenith angle of 0^o ($\lambda\lambda$ 2000-8000Å); the results are shown by the solid curve in Figure 25. The dotted portion of this curve below about 2500Å represents a crude extrapolation to reflect the fact that CO_2 begins to absorb for $\lambda\lambda < 1975$Å,[63] so that these radiations are precluded from striking the Martian surface with any significant intensity. The heavy dashed curve in Figure 25 represents the corresponding background conditions which prevail for an Earth-based platform (note that two scales are employed in the figure). This composite presentation makes evident two important factors. First, for $\lambda\lambda$ 3000-8000Å background intensities encountered at the Martian surface are about two orders of magnitude less than those on Earth, (this is roughly equivalent to a platform placed at 30 km above the surface of the Earth) and second, it becomes evident that the observational spectral range can be extended down to 2000Å for the case of Mars. However, at this point a word of caution should be injected. Some of this apparent improvement in background

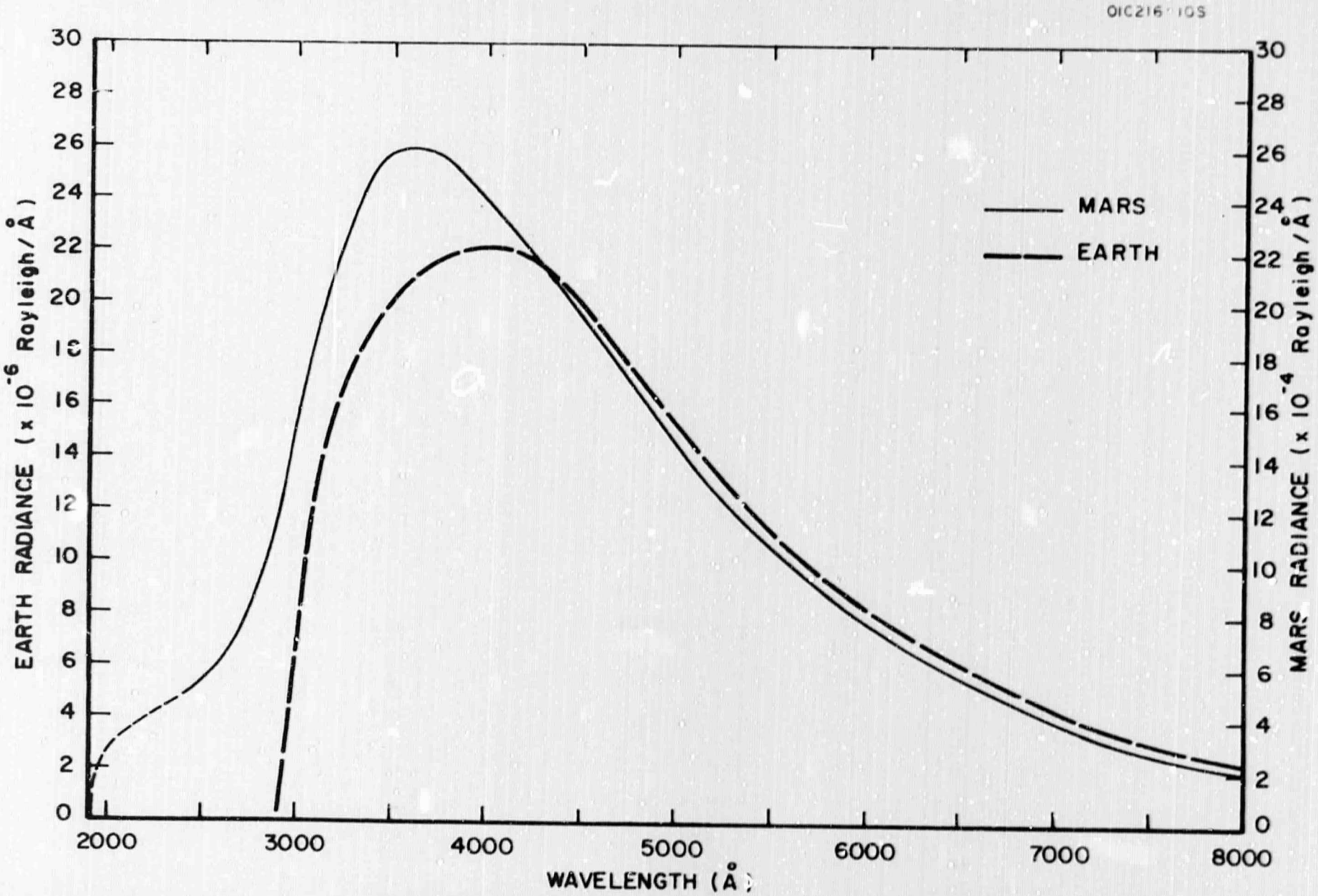

Figure 25. Zenith sky radiance for solar zenith angle of zero degrees.

radiation was due to the scaling factor involved in the incident flux, thus for those signal sources which depend upon the solar flux, a corresponding decrease would be involved. On the other hand, for the case of self-emission processes full advantage of the background conditions can be achieved. In addition, the presence of certain minor constituents can effect the region λλ 2000-3000Å. Furthermore, it should be stressed that only the role of Rayleigh scattering has been considered here so that the presence of a solar illuminated surface haze layer would result in a Mie scattering background intensity not accounted for here.

According to Figure 25, relatively strong signal sources would be required for positive identification even against the greatly reduced Martian surface intensities. However, both the difficulties of the possible haze layer and the required strong signal sources can be significantly minimized by the performance of twilight experiments. Some of the salient features and advantages of performing such experiments have been examined in some detail as described below.

b. <u>General Considerations Pertinent to Twilight Airglow Observations Performed on a Mars Lander Platform</u>.

At this point, it is convenient to tabulate some selected planetary and orbital data for Earth and Mars. These are given in Table 2 below.

TABLE 2

	Earth	Mars
Equatorial Radius (km)	6378	3380
Axial Rotation Period	$23^h56.07^m$	$24^h37.38^m$
Sidereal Period of Revolution (days)	365.26	686.98
Semi-major Axis (A.U.)	1.000	1.524
Orbital Inclination to Ecliptic (deg)	0.00	1.85
Inclination of Equatorial to Orbital Plane (deg)	23.45	23.98

The remainder of this report will involve (a) the calculations of shadow height, h, vs. solar depression angle (SDA), α, for the planet Mars, (b) the estimation of the corresponding zenith sky radiance for various SDA values, and finally (c) the determination of the time duration of twilight for a number of selected latitudes on the planet Mars.

The geometry for twilight observations in planetary atmospheres has been discussed in detail by Chamberlain.[64] The present estimates have been obtained for the simplified case where atmospheric refraction and absorption are neglected so that a sharp shadow height line h, prevails. Under these conditions, Chamberlain[64] has shown that for small SDA for the planet Earth

$$h \simeq \frac{R\alpha^2}{2} \tag{12}$$

$$h = 6378\ \alpha^2/2(57,30)^2 \tag{13}$$

or

$$h \simeq \alpha^2. \tag{14}$$

Additionally, according to Table 2, it then follows that for the case of Mars (R = 3380 km).

$$2h \simeq \alpha^2 \tag{15}$$

Figure 26 gives the shadow line altitude vs. SDA relationship for the planets Earth and Mars whereas in Figure 27 are shown the calculated zenith sky radiances for $\lambda\lambda$ 2000-8000Å for various SDA values on Mars. (The corresponding shadow height values are included along with the several indicated α-values.) Here again as in Figure 25, the dotted portion in the vicinity of 2000Å represents a crude extrapolation owing to the absorption of CO_2 for $\lambda\lambda < 1975$Å. When the radiance curves in Figure 27 are compared

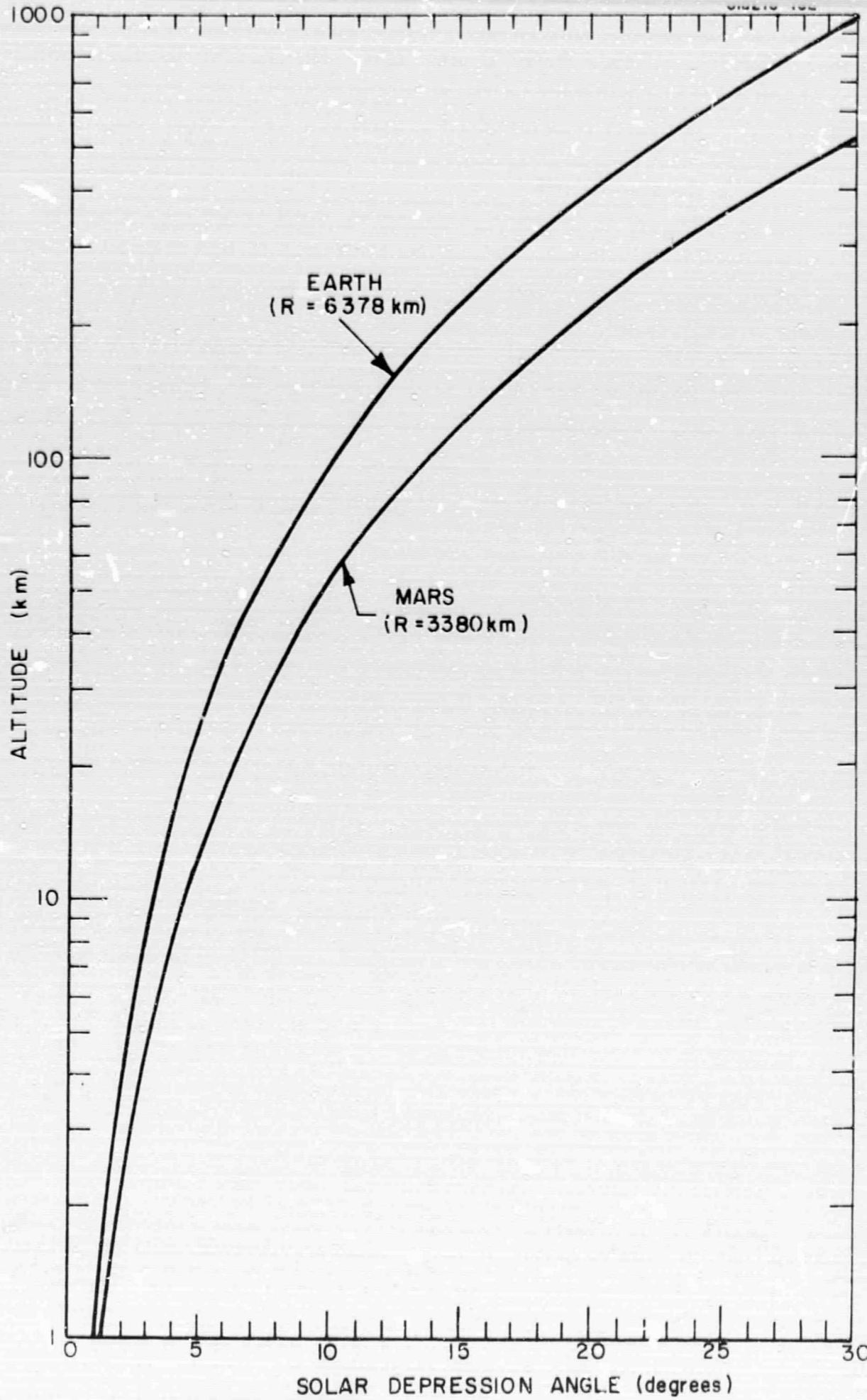

Figure 26. Shadow height, h, as a function of solar depression angle, α, for the planets Earth and Mars.

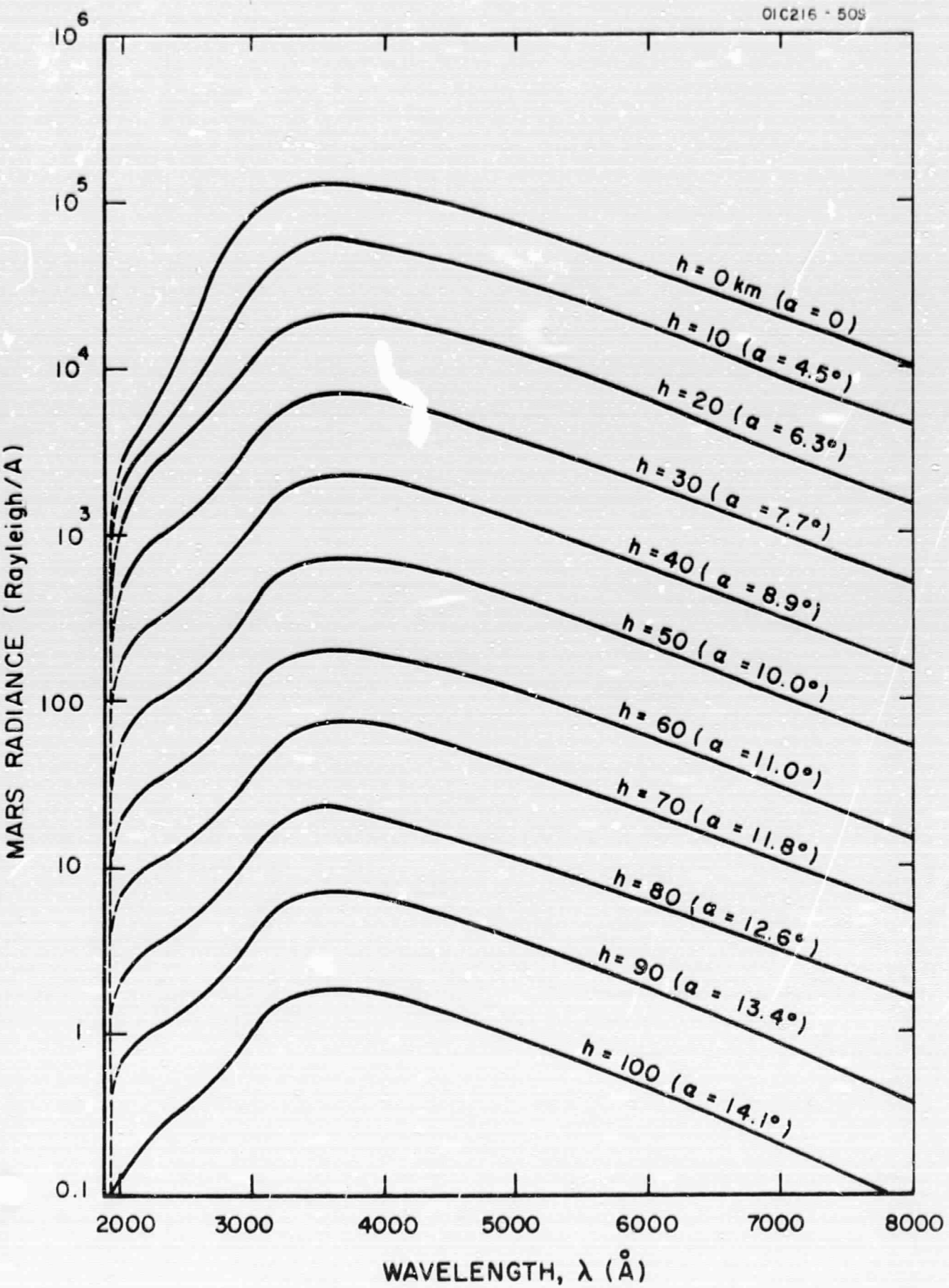

Figure 27. Zenith sky radiance for various solar depression angle for Mars.

to the corresponding data for an Earth-based platform, it becomes evident that in all cases for a given shadow height the background intensity is considerably reduced. This behavior is even more evident for lower h-values where the need for such imprpvement is generally greatest.

As a final task, estimates were obtained for the time duration of specific twilight conditions which obtain on both Earth and Mars in order to be available for future comparison. For the present purpose, twilight is defined for a change in SDA from $0\text{-}18^{o}$ (which corresponds to astronomical twilight). Specifically, then, the time durations (of this twilight condition) as a function of date at common latitudes were acquired for both planets. The data, pertinent to the case of Earth was deduced directly from data contained in the American Ephemeris and Nautical Almanac. On the other hand, corresponding data for Mars are not readily available; in this case, they were calculated by the following expression

$$\Delta t_T = \left| \frac{\tau_o - \tau_T}{360/24.7} \right| \qquad (16)$$

Δt_T = time duration for astronomical twilight = $\Delta\alpha = 0\text{-}18^{o}$, $\cos \tau_o = -\tan \delta \tan \lambda$.

$$\cos \tau_T = - \frac{\sin \delta \sin \lambda + \sin \alpha}{\cos \delta \cos \lambda} \qquad (17)$$

where

δ = solar declination angle

λ = geographic latitude

and α = solar depression angle

The factor 360/24.7 relates to the rotation period pertinent to Mars.

The time duration of astronomical twilight ($\Delta\alpha$ = 0-18°) for the northern hemisphere of Earth and Mars are shown in Figures 28 and 29 respectively; the similarity of the Δt_T-values for common latitudes is striking. This behavior reflects the planetary and orbital characteristics shown in Table 2.

In summary then, the following features have been noted: (a) For the spectral region $\lambda\lambda$ 3000-8000Å, the zenith sky radiance on the surface of Mars is about two orders of magnitude less than that which prevails on the surface of the Earth. (This corresponds to a platform at 30 km above the Earth's surface.) (b) For Mars, the spectral region of investigation can be extended down to $\lambda\lambda \cong$ 2000Å. (c) The time duration of specified twilight conditions for Earth and Mars are similar. (d) For given SDA-values, the shadow height on Mars is about 1/2 of that corresponding value for Earth. This affords the opportunity of increased observation time per unit altitude interval, and (e) on Mars longer seasons prevail; this affords more optimum experimental opportunity.

During the next phase of this study, these various features will be exploited with an aim to deriving maximum advantage in performing Mars lander dayglow experiments.

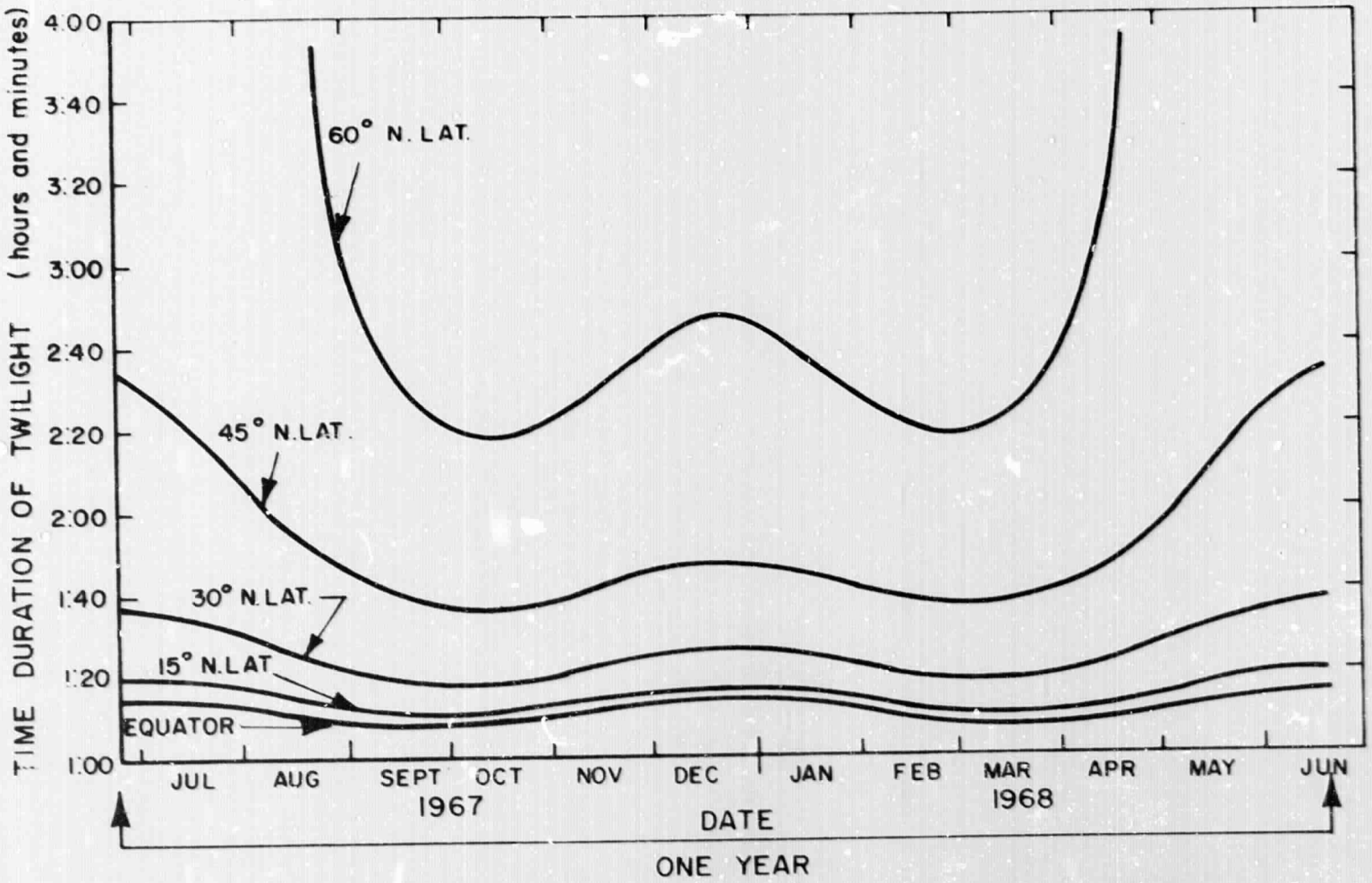

Figure 28. Time duration of twilight ($\Delta\alpha = 18^{o}$) for Earth

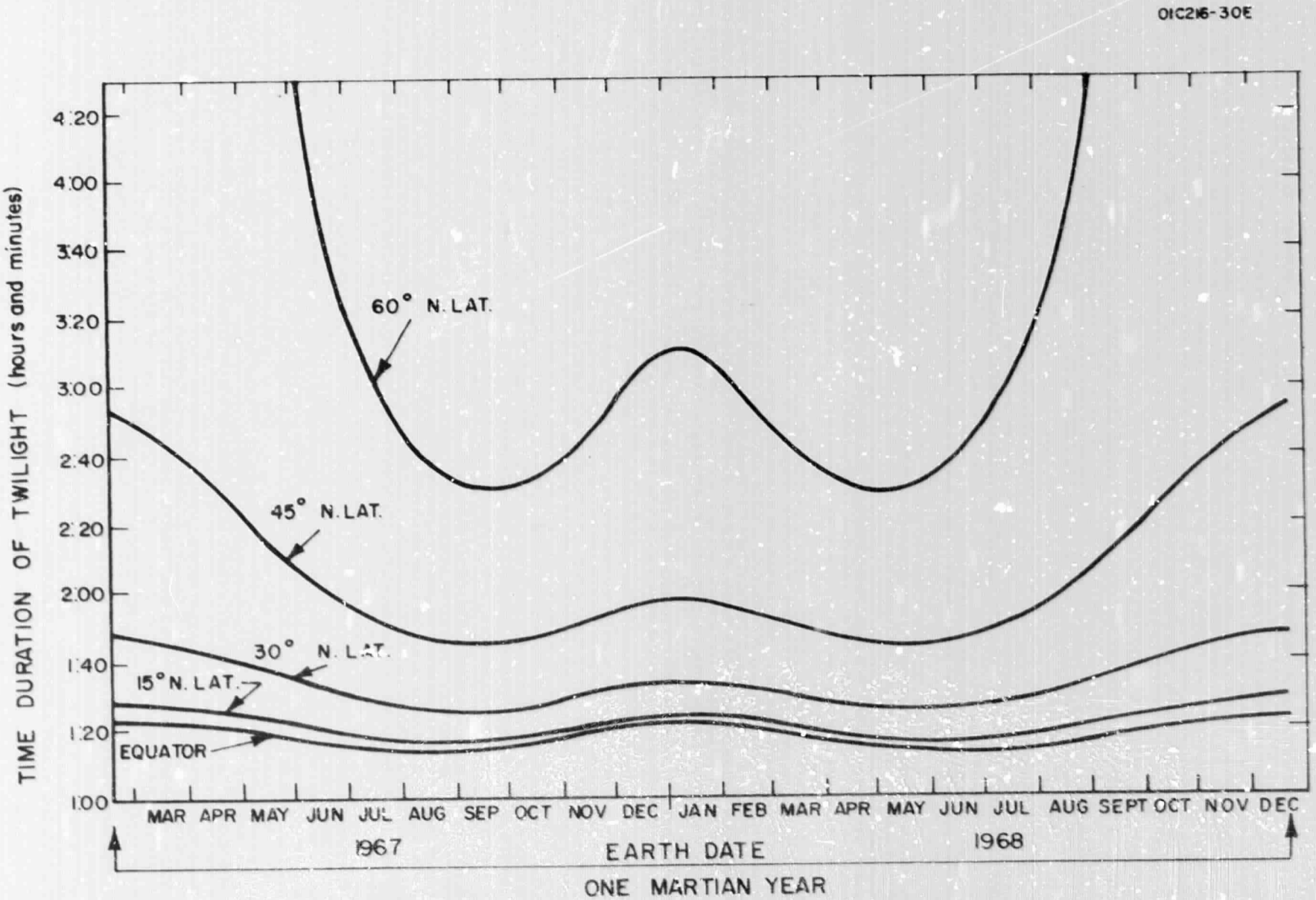

Figure 29. Time duration of twilight ($\Delta\alpha$ = 18°) for Mars.

III. MISCELLANEOUS TOPICS

This section contains brief summaries of the scientific material generated under the present program and presented at scientific and/or professional meetings. In addition, there is included other miscellaneous topics of interest in the performance of the current contract committments.

During the current reporting period, Dr. James A. R. Samson attended the IAGA symposium on "Laboratory measurements of Aeronomic Interest" held at the University of York, Toronto during 3-4 September 1968 and also to visit the laboratories of Dr. Marmet at the University of Laval, Quebec City, Canada.

Of particular interest to the present contract was the paper presented by Dr. R. Schoen on Photoelectron Spectroscopy, Photoionization and Photoabsorption measurements. He pointed out that the absorption cross sections of CO_2 vary widely from observer to observer and although he believed the values obtained at GCA were the best available he felt they should be remeasured. He also brought up the importance of the angular distribution of the photoelectrons in photoelectron spectroscopy experiments. Independently of the work produced at GCA, he also arrived at the look angle of 54° 44' for observations in order to eliminate any confusion of the results due to varying angular distributions.

McElroy brought out the fact that the abundance of atomic nitrogen produced by dissociative ionization appears to be too small to account for what he expects to exist in the upper atmosphere. The discussions on this point suggested that electron impact collisions with N_2 may be the major instrument for producing dissociative ionization.

Dr. Hoffman of the AFCRL, gave an excellent review of the present state of absorption cross sections of atmospheric gases and pointed out the need for continued measurements at higher wavelength resolution.

At Laval University, Dr. Marmet described his new ideas for measuring the kinetic energies of photoelectrons. His new analyzer is basically a 127° cylindrical deflection analyzer with a modification to provide a higher transmission of electrons. The device looks extremely promising for photoelectron work. However, it has not been tested as yet and we propose to hold off making this type until such time that Dr. Marmet has more information on its energy resolution and other characteristics. Dr. Marmet has had many years of experience dealing with electron and ion optics and he was able to provide unvaluable suggestions about the techniques in working with electrons, especially in methods to remove local magnetic fields.

REFERENCES

1. Samson, J. Opt. Soc. Am. 54, 6 (1964).

2. Canfield, L. R., Johnson, R. G., Codling, K. and Madden, R. P., Appl. Optics 6, 1886 (1967).

3. Samson, J. A. R. in Advances in Atomic and Molecular Physics, Eds. Bates, D. R. and Estermann, I. (Academic Press, New York, 1966) Vol. 2, p. 177.

4. Samson, J. A. R. and Cairns, R. B., Phys. Rev. 173, 80 (1968).

5. Manson, S. T. and Cooper, J. W., Phys. Rev. 165, 126 (1968).

6. Lotz, W., Astrophysical J. Suppl. Series 14, 207 (1967).

7. Dalgarno, A., McElroy, M. B. and Walker, J. C. G., Planet. Space Sci. 15, 331 (1967).

8. Dalgarno, A. and Walker, J. C. G., Planet. Space Sci. 15, 200 (1967).

9. See for example D. W. Turner and D. P. May, J. Chem. Phys. 45, 471 (1966); R. Spohr and E. Van Puttkamer, Z. Naturforsch. 22a, 705 (1967); J. Berkowitz, H. Ehrhardt and T. Tekaat, Z. Physik 200, 69 (1967).

10. Frost, C., McDowell, C. A. and Vroom, D. A., Proc. Roy. Soc. 296, 566 (1967).

11. Hamm, R. MacRae, and E. Arakawa, J. Opt. Soc. Am. 55, 1460 (1965).

12. Cooper, J. and Zare, R. N., J. Chem. Phys. 48, 942 (1967).

13. Cooper, J. and Zare, R. N., in Lectures in Theoretical Physics (Gordon and Breach, Inc., New York, to be published) Vol. XI.

14. Lipsky, L., Phys. Rev. (to be published).

15. Cooper, J. W. and Manson, S. T., Phys. Rev. (to be published).

16. Sun, H. and Weissler, G. L., J. Chem. Phys. 23, 1160 (1955).

17. Watanabe, K., Zelikoff, M. and Inn, E. C. Y., AFCRL Tech. Rept. No. 53-23, Geophys. Res. Paper No. 21 (1953).

18. Wilkinson, P. G., Can. J. Phys. 34, 596 (1956).

19. Dalgarno, A. and Degges, T. C., Planet. Space Sci., 16, 125 (1968).

20. Evans, J. V., Planet. Space Sci. 13, 1031 (1965).

21. Evans, J. V., Planet. Space Sci. 15, 1387 (1967).

22. Evans, J. V., J. Geophys. Res. 72, 3343 (1967).

23. Carru, H., Petit, M. and Waldteufel, P., J. Atmos. Terr. Phys. 29, 351 (1967).

24. Petit, M., Compt. Rend. Acad. Sci. Paris 264B, 1530 (1967).

25. Petit, M., Ann. Geophys. 24, 1 (1968).

26. Farley, D. T., McClure, J. P., Sterling, D. L. and Green, J. L., J. Geophys. Res. 72, 5837 (1967).

27. Mahajan, K. K., J. Atmos. Terr. Phys. 29, 1137 (1967).

28. Dalgarno, A., McElroy, M. B. and Moffett, R. J., Planet. Space Sci. 11, 463 (1963).

29. Donahue, T. M., Ann. Geophys. 22, 175 (1966).

30. Hinteregger, H. E., Hall, L. A. and Schmidtke, G. in Space Research V, p. 1175, North-Holland, Amsterdam (1965).

31. Dalgarno, A., Henry, R. J. W. and Stewart, A. L., Planet. Space Sci. 12, 235 (1964).

32. Comes, F. J., Speier, F. and Elzer, A., Z. Naturforsch. 23a, 125 (1968).

33. Cairns, R. B. and Samson, J. A. R., Phys. Rev. 139, A1403 (1965).

34. Henry, R. J. W. and McElroy, M.B. in The Atmospheres of Venus and Mars (ed. J. C. Brandt and M.B. McElroy), Gordon and Breach, New York (1968).

35. Henry, R. J. W., Planet. Space Sci. 15, 1747 (1967).

36. Stewart, A. I., Private communication (1968).

37. Hanson, W. B. in Space Research III, North Holland, Amsterdam, p. 282, (196).

38. Geisler, J. E. and Bowhill, S. A., J. Atmos. Terr. Phys. 27, 457 (1965).

39. Carlson, H. C., J. Geophys. Res. 71, 195 (1966).

40. Hanson, W. B. and Cohen, R., J. Geophys. Res. 73, 831 (1968)

41. Hanson, W. B. and Johnson, F. S., Memoires Soc. R. Sc. Liege, Ser. 5, 4, 390 (1961).

42. Watanabe, K. and Hinteregger, H. E., J. Geophys. Res. 67, 999 (1962).

43. Spitzer, L., in Physics of Fully Ionized Gases, Interscience Publishers, Inc., New York (1956).

44. Banks, P. M., Planet. Space Sci. 15, 77, (1967).

45. Holmes, J. C., Johnson, C. Y. and Young, J. M., in Space Research V, p. 756, North-Holland, Amsterdam (1965).

46. Taylqr, H. A., Jr., Brace, L. H., Brinton, H. C. and Smith, C. R., J. Geophys. Res. 68, 5339 (1963).

47. Walker, J. C. G. and Rees, M. H., Planet. Space Sci. 16, in press, (1968).

48. Banks, P., Planet. Space Sci. 14, 1085 (1966).

49. Dalgarno, A. and Henry, R. J. W., Proc. Roy. Soc., London, A288, 521 (1965).

50. Hake, R. D., Jr. and Phelps, A. V., Phys. Rev. 158, 70 (1967).

51. Mentzoni, M. H. and Row, R. V., Phys. Rev. 130, 2312 (1963).

52. Rees, M. H., Walker, J. C. G. and Dalgarno, A., Planet. Space Sci. 15, 1097 (1967).

53. Banks, P. M., Planet. Space Sci. 14, 1105 (1966).

54. Rees, M. H. and Walker, J. C. G., Ann. Geophys. 24, 193 (1968).

55. Walker, J. C. G. and Rees, M. H., Planet. Space Sci. 16, 459 (1968).

56. Banks, P. M., Earth Planet. Sci. Letters 1, 270 (1966).

57. Banks, P. M., J. Geophys. Res. 72, 3365 (1967).

58. Marmo, F. F., "Experimental and Theoretical Studies in Planetary Aeronomy"9th Quarterly Progress Report, GCA Technology Division, Bedford, Massachusetts (June, 1967)

59. Johnson, F. S., J. Meteorology 11, 431 (1954).

60. Dalgarno, A., Degges, T. C. and Williams, D. A. Proc. Phys. Soc. (London) 92, 291 (1967).

61. Condon, E. V. and Odishaw, H., Handbook of Physics, Second Edition, McGraw-Hill Book Co. (1967).

62. Evans, D. C., Science 149, 969 (1965).

63. Harteck, P., Reeves, R. R. and Thompson, B. A., "Photochemical Problems of the Venus Atmosphere" NASA TN-D1984 (1963).

64. Chamberlain, J. W., Physics of the Aurora and Airglow, Academic Press, New York (1961).